DIRECT GROWTH OF CARBON NANOTUBES ON INCONEL SHEETS USING HOT FILAMENT CHEMICAL VAPOR DEPOSITION

A Thesis Submitted to the
College of Graduate Studies and Research
in Partial Fulfillment of the Requirements
for the degree of Master of Science
in the Department of Mechanical Engineering
University of Saskatchewan
Saskatoon

By
Wenwen Yi

PERMISSION TO USE

In presenting this thesis in partial fulfilment of the requirements for a Postgraduate degree from the University of Saskatchewan, I agree that the Libraries of this University may make it freely available for inspection. I further agree that permission for copying of this thesis in any manner, in whole or in part, for scholarly purposes may be granted by the professor who supervised my thesis work or, in her absence, by the Head of the Department or the Dean of the College in which my thesis work was done. It is understood that any copying or publication or use of this thesis or parts thereof for financial gain shall not be allowed without my written permission. It is also understood that due recognition shall be given to me and to the University of Saskatchewan in any scholarly use which may be made of any material in my thesis.

Requests for permission to copy or to make other use of material in this thesis in whole or part should be addressed to:

Head of the Department of Mechanical Engineering
57 Campus Drive
University of Saskatchewan
Saskatoon, Saskatchewan
Canada
S7N 5A9

ABSTRACT

Carbon nanotubes (CNTs) have great potential in many applications due to their unique structure and properties. However, there are still many unsolved problems hampering their real applications. This thesis focuses on three important issues limiting their applications, namely: (1) direct growth of CNTs without additional catalyst, (2) secondary growth of carbon nanotubes on primary CNT bed without using extra catalyst, (3) and CNT alignment mechanisms during the growth.

The CNTs used in this thesis were prepared by hot filament chemical vapor deposition (CVD) reactor and characterized using scanning electron microscopy (SEM), transmission electron microscopy (TEM), X-ray diffractometry (XRD), and Raman spectroscopy. Field electron emission (FEE) properties of the CNTs were also tested.

Oxidation-reduction method was adopted in direct growth of CNTs on Inconel 600 plates and proved effective. The effect of oxidation temperature on the growth of CNTs was studied. It was found that the oxidation temperature had an influence on CNT height uniformity and FEE properties: the higher the treatment temperature, the more uniform the resultant CNTs, and the better the FEE properties of the resultant CNTs. The contribution of different oxides formed at different temperatures were investigated to explain the effect of oxidation temperature on the CNT height uniformity.

Secondary CNTs were grown on primary ones by simply changing the carbon concentration. No additional catalyst was used during the whole deposition process. It was found that synthesizing primary CNTs at extremely low carbon concentration is key factor for the secondary growth without additional catalyst. The CNT sample grown with secondary nanotubes exhibited improved field emission properties.

The effect of bias voltage on growth of vertically aligned carbon nanotubes was investigated. The CNTs grown at -500V shows the best alignment. At the early growth stage, simultaneous growth of randomly oriented and aligned carbon nanotubes was observed. This was consistent with the alignment mechanism involving stress that imposed on cat-

alyst particles on tube tips. Through the observation of CNT growth on the scratched substrates, catalyst particle size was found as another determining factor in the alignment of CNTs. Big catalyst particles promoted aligned growth of CNTs.

ACKNOWLEDGEMENTS

The following thesis has been made possible owing to the help, support, and inspiration of many people. In the first place, I am very grateful to my supervisor, Dr. Qiaoqin Yang, who has supported me with constant encouragement and invaluable directions at every stage of the thesis process. I would also like to express my sincere thanks to my thesis supervisory Committee: Dr. Chris Zhang, Dr. Qiaoqin Yang, and Dr. Ike Oguocha. Their patience and insights on research always inspired me to pursue the excellence without compromise.

Next, I would like to thank the help from all my colleagues: Songlan Yang, Yongji Tang, Longshan Xu, Jingang Yu, Munan Yu, Zhouyi Hu, Haidong Wang. The discussion and cooperation with them contributed substantially to the completion of this work. I am also indebted to the manager of materials labs, Rob Peace.

I must express my sincere gratitude to Professor Akira Hirose and his crews in Plasma Physics Laboratory, University of Saskatchewan. All of the deposition works and field emission tests were done in this lab. I have received generous help from many people in technical and instrumental aspects. Here, I would like to thank Dr. Chijin Xiao, David McColl, Yuanshi Li, and Tianye Niu. I am also indebted to Tom Bonli in Electron Microscopy Laboratory (University of Saskatchewan-Geology). I appreciate his help with Scanning Electron Microscopy observation and X-ray diffraction measurements.

Equally important help has been provided to my life by my friends: Yan Li, Yang Lin, Qingshu Zhang, Ruizhi Luo, Yang Si, and Xiaohui Bao. Life in Saskatoon would not be so exciting without them. Special thanks go to my boyfriend Bo Yu, who always stands by me and has witnessed my every growing-up step in the past more than two years.

Finally, I would like to thank my family for their everlasting support.

To my parents and my sister.

CONTENTS

LIST OF TABLES

LIST OF FIGURES

List of Abbreviations

AAO	Anodic aluminum oxide
BSE	Backscattering electrons
CVD	Chemical vapor deposition
CCVD	Catalytic chemical vapor deposition
CNT	Carbon nanotube
CNF	Carbon nanofibre
DC-PECVD	Direct current-plasma enhanced chemical vapor deposition
ECR-PECVD	Electron cyclotron resonance-plasma enhanced chemical vapor deposition
EDS	Energy-dispersive X-ray spectroscopy
EELS	Electron energy loss spectrometry
FEE	Field electron emission
FEF	Field enhancement factor
FET	Field effect transistor
FN	Fowler-Nordheim
HFCVD	Hot filament chemical vapor deposition
ICP-PECVD	Inductively coupled plasma enhanced chemical vapor deposition
M-PECVD	Microwave-plasma enhanced chemical vapor deposition
MWCNT	Multi-walled carbon nanotube
PECVD	Plasma enhanced chemical vapor deposition
RF-PECVD	Radio frequency-plasma enhanced chemical vapor deposition
SEI	Secondary electron imaging
SEM	Scanning electron microscope
SFM	Scanning-force microscopy
SPM	Scanning probe microscopy
STEM	Scanning transmission electron microscope
SWCNT	Single-walled carbon nanotube
TCVD	Thermal chemical vapor deposition
TEM	Transmission electron microscope
WDS	Wavelength-dispersive X-ray spectroscopy
XRD	X-ray diffractometry
CRT	Cathode Ray Tube

LIST OF SYMBOLS

$\vec{C}$	A vector in graphite plane
$\vec{a_1}$	Graphite vector
$\vec{a_2}$	Graphite vector
σ	σ bond
π	π bond
I	Emission current
J	Emission current density
A	Notional emission area
ϕ	Local work function
E	Applied electric field, kinetic energy of electron
V	Applied voltage
d	Probe-sample distance
β	Field enhancement factor
F	Local electric field
a	Universal constant
b	Universal constant
υ_N	Nordheim function
t_N	Nordheim function
α	Effective emission area
λ	Wavelength of the X-rays

CHAPTER 1

INTRODUCTION

1.1 Motivation

Carbon nanotubes (CNTs) hold great potential for many applications due to their unique structure and properties. Stimulated by their wide potential applications, a large number of works have been done and significant progress has been made in the synthesis of CNTs [1]. Nonetheless, to realize the full potential of their practical applications, several challenges remain to be addressed. These include direct growth of CNTs without additional catalyst and controlled growth of well-aligned CNTs. In recent years, much effort has been put to overcome these challenges and the progress that has been made can be summarized as follows:

- To create nano-sized catalyst particles in-situ on the substrate surface other than pre-coating catalyst is considered to be the key to deposit CNTs directly on metal substrate using chemical vapor deposition (CVD). Up to now, several techniques have been tried to grow CNTs directly on Fe [2], Ni [2, 3], and Ni containing alloys (stainless steel (SS) [4–8], Inconel [3, 9–12]). One of them was using plasma to produce catalytic sites in-situ for CNT growth [2, 4, 7–10]. Some made use of liquid catalyst to produce floating catalytic particles to facilitate the CNT growth [11, 12]. Oxidation-reduction pre-treatment was also used to prepare particles of catalyst directly from the alloy substrates and the growth of CNTs on the pre-treated substrates has been reported [3, 5, 6] in which alloy substrates were first oxidized in air and then reduced in H_2 before the thermal CVD process. However, the effect of the pretreatment temperature on the formation of oxides and thus the quality of the resultant

CNTs was not investigated.

- It has been found that the growth of secondary CNTs can enlarge the surface area of the primary tubes remarkably, which is significant in applications of biological sensors and field emitters. To generate secondary CNTs, particulate Ni or Fe catalysts were electrodeposited [13–15], or sputtered [16], or electron beam evaporated [17] onto primary CNTs; or the synthesized CNTs were dipped into ferritin solution [16] and then dried in air to form particles of catalyst on CNT bed. The CVD process was then applied for secondary growth. Secondary CNT growth without the addition of extra catalyst has not been reported.

- Aligned CNTs have been synthesized by using (i) thermal CVD on porous silicon embedded with catalyst nanoparticles [18, 19]; (ii) van der Waals forces between neighboring tubes when a very dense catalyst distribution was applied [20]; (iii) plasma [21]; and (iv) electric field without plasma [22]. Due to the possibility of large-scale controlled growth at relatively low temperature, plasma enhanced CVD growth of aligned carbon nanotubes have been widely studied and different CNT alignment mechanisms have been proposed. Merkulov *et al*. [23–25] proposed a stress induced alignment mechanism from glow discharge plasma enhanced chemical vapor deposition (PECVD) of aligned carbon nanotubes. Bower *et al*. [21, 26] proposed an alignment mechanism which emphasizes the self biasing effect induced by plasma in microwave plasma enhanced chemical vapor deposition (MPECVD) system. Ren *et al*. [27, 28] adopted plasma enhanced hot filament chemical vapor deposition (PE-HFCVD) method to successfully fabricate large–scale well aligned carbon nanotubes. However, the alignment mechanism was not given. Chen *et al*. [29, 30] suggested the effect of directional electrical force in aligning the CNTs during PE-HFCVD process. This mechanism has been supported by many other researchers on PE-HFCVD synthesis of aligned CNTs. In my thesis, however, simultaneous growth of random and aligned CNTs has been observed in the early growth stage using DC PE-HFCVD, which is not in agreement with Chen's theory and needs to be further investigated.

1.2 Objectives

This thesis aimed to address the aforementioned challenges in the synthesis of CNTs. Specifically, the objectives of this research project were:

1. To use oxidation-reduction method to create catalytic site in-situ to achieve direct growth of CNTs on Inconel 600 sheets.

2. To achieve secondary CNTs growth without addition of catalysts by changing growth parameters .

3. To apply bias voltage on substrates to control the alignment of CNTs.

4. To optimize growth conditions to synthesize CNTs with much superior FEE properties for FEE applications.

1.3 Methodology

Hot filament chemical vapor deposition (HFCVD) technique was employed to synthesize carbon nanotubes, while a variety of techniques was used to characterize the synthesized carbon nanotubes, including scanning electron microscopy (SEM), transmission electron microscopy (TEM), Raman spectroscopy, X-ray diffractometry (XRD), and field electron emission. SEM allows for the ropes of single-walled nanotubes (SWNTs) in a sample to be imaged [31] or the highly oriented forest of multiwalled carbon nanotubes (MWNTs) to be viewed [32]. Although the resolution of this technique does not allow one to image individual SWNTs within an SWNT bundle, combined with other techniques it can be used to determine the amount of impurities present such as amorphous carbon or carbon-coated catalyst particles, which typically co-exist with SWNT bundles in the sample [33]. TEM is a powerful high- resolution technique which allows one to determine the number of walls in the MWNT [32, 34] or image the isolated SWNTs residing inside a SWNT bundle. It has the capacity for accurate measurement of tube diameters as well as investigation of structural defects within CNTs. TEM has also played an important role

in investigating new structures such as SWNT peapods [35] and the effects of nitrogen doping in MWCNTs [36]. Raman spectroscopy is also a very powerful technique for analyzing carbon materials. It can be used to differentiate SWCNTS and MWCNTS, diamond and graphitic structures [37] and to determine the diameter, chirality, dopants, and intercalation properties of SWCNTS [38]. XRD is usually used to study the formation of carbon structures [39], however, it can not alone confirm the formation of CNTs. XRD is also used to identify the catalyst materials for CNT growth and distinguish between SWCNT and MWCNT [40]. CNTs are suitable for field electron emitters due to their electrical conductivity, nano-scale dimension, and high aspect ratio. Thus the field electron emission (FEE) properties of the synthesized CNTs were also characterized using Keithley 237 test unit.

1.4 Organization of the thesis

This thesis is organized as follows. Chapter 1 consists of the motivation, objectives, and methodology of the thesis. Chapter 2 gives a detailed literature review including the properties, applications, and synthetic techniques of carbon nanotubes. Particularly, aligned and direct growth as well as the field electron emission theories have been addressed. Experimental methodologies have been described in Chapter 3, including the CVD reactor and growth parameters for CNT synthesis and the techniques for characterization. Chapter 4 presents the results and discussion including the effect of substrate oxidation temperature on the deposition of carbon nanotubes directly on Inconel sheets, the effect of gas composition on CVD deposition of CNTs, and the aligned growth of carbon nanotubes using plasma enhanced CVD. Chapter 5 summarizes the main results of the thesis work and provides some suggestions for the future work.

CHAPTER 2

LITERATURE REVIEW

2.1 Properties and Applications of carbon nanotubes

A carbon nanotube (CNT) is a hollow tube structure formed of rolled graphene strips. Because of its unique one dimensional structure, it possesses many outstanding properties and thus a wide range of potential applications. Therefore, great effort has been put into the investigation of synthesis and applications of CNTs since its discovery in 1991 by Iijima [41]. In this section, various properties and the corresponding applications of carbon nanotube will be reviewed.

2.1.1 Electronic properties and corresponding applications

A single-walled carbon nanotube (SWCNT) is briefly a rolled up graphene strip. As such, it is easy to understand that the rolling manner determines its structure. The circumferential periodicity of a SWNT can be specified by a pair of integers (n, m) that denotes a vector $\vec{C}$ ($\vec{C} = n * \vec{a_1} + m * \vec{a_2}$, $\vec{a_1}$ and $\vec{a_2}$ are graphite vectors) [42]. The two ends of vector C are rolled onto each other when forming a tube. Theoretical predictions have shown the close relationship between CNT structure and its electronic properties [43–45]. Carbon nanotubes have either metallic or semiconducting characteristics, depending on the diameter and the indices (n, m). Particularly, confine effect on the tube circumferences makes individual metallic tubes or metallic tube ropes behave like quantum wires [46–48]. These extraordinary electronic properties are essential to carbon nanotubes in their electronic applications. For example, joining two half-tubes of different helicity would make nanoscale metal-semiconductor, or semiconductor-semiconductor, or metal- metal junc-

tions [49–51], respectively. These nanoscale junctions are of great significance in building nanoscale electronic devices. Impurities and defects were also found to have certain impact on the conductance of the metallic nanotubes [52]. Therefore, doping is often adopted in applications of carbon nanotubes in semiconductor device. CNT–based molecular electronics mainly include field emission devices [53] and field effect trasistor (FET) [54, 55]. Besides individual nanotubes, nanotube ropes and crossed–tube junctions have also been investigated [56]. The intertube interactions give rise to many potential applications, for example, nanotube memory. Moreover, mechanical, chemical, biological, thermal, and magnetic interactions with nanotubes can affect their electronic properties, leading to many extended applications that will be introduced in the following sections.

2.1.2 Mechanical, electromechanical properties and corresponding applications

Since CNT is intrinsically a rolled graphite sheet, bonding in nanotubes is sp^2 formed by three in-plane σ bonds and an out-of-plane π bond [57]. Owing to the strong short σ bonding, carbon nanotube exhibits the highest Young's modulus and tensile strength among all the materials. Theoretical [58, 59] and experimental data [60–62] show Young's modulus as high as 1 TPa for SWCNT, and 1.1 to 1.3 TPa for multi-walled carbon nanotubes (MWCNT). The robust mechanical properties and high aspect ratio make carbon nanotube an ideal probe material in scanning probe microscopy (SPM) [63] and scanning-force microscopy (SFM) [64]. These tools may be exlusively used in information technology and biological science due to the inherent mechanical flexibility of nanotube probes. As discussed in section 2.1.1, the electronic properties of CNTs have high sensitivity to their structure. Thus it is not surprising to find changes in electronic properties of asymmetric tubes when they undergo a tensile or torsional strain. There are mainly two kinds of resultant electromechanical effects. One is the metal-insulator transition caused by mechanical deformation, namely, piezoresistance [65–67]. The other effect is electromechanical actuator [68], in which a voltage is applied to bring in mechanical deformation. Combined with the mechanical properties, these electromechanical effects may lead to the develop-

ment of nanotube-based mechanical sensors and actuator, and even more complex devices such as oscillators or electromechanical switches.

2.1.3 Optical, optoelectronic properties and corresponding applications

It is generally known that excitations of electrons or holes from one energy level to another cause optical transition. Optical and optoelectronic properties of carbon nanotubes are thus dependent on their band and sub band structures that are decided largely by tube diameter and chirality. Resonant Raman [69], and fluorescence [70] have been extensively used to study the electronic structure of nanotubes by analyzing the position and intensity of the peaks of the spectra. These spectra can also help to determine the orientation of tubes since the intensity of optical transition is much greater when the polarized light is parallel to the tube axis than when it is not. Well–defined band and sub band structures of nanotubes are of essential importance in applications such as optical and optoelectronic devices. In particular, semiconducting nanotubes have a theoretically predictable ability to emit light of wavelength ranging from 300 to 3000 nm, which is ideal for IR detectors [71]. Electronically induced light emission of wavelength of 1500 nm was experimentally observed from semiconducting carbon nanotubes [72].

2.1.4 Magnetic, electromagnetic properties and corresponding applications

Carbon nanotubes have similar magnetic properties as graphite, e.g. anisotropic magnetic susceptibilities [73]. As such, both single-walled and multi-walled carbon nanotubes have been successfully aligned by external magnetic fields [74, 75]. Another interesting property of carbon nanotubes is their electrical response to a magnetic field. Because the band gap of nanotube change with the applied magnetic field, metallic–semiconducting transition has been realized [76]. This unique property will lead to interesting applications of carbon nanotubes in information storage devices.

2.1.5 Chemical, electrochemical properties and corresponding applications

Carbon nanotubes have higher chemical and biological activity than graphite owing to the circular curvature and σ - π rehybridization. In particular, CNT ends are more reactive than the sidewalls because of the greater curvature and the existence of pentagons on the open ends [77]. Therefore, a variety of functional groups can be attached to the open ends and/or sidewalls to modify the properties of CNTs. Although not soluble in water, carbon nanotubes can be wetted by various solvents and oxides, thereby leading to meaningful applications like separating insoluble impurities [78]. In addition, capillary effect makes it possible to fill different agents into the interior hollow space of the CNTs [79] and thus enhancing the fabrication of CNT–reinforced composites. Adsorption is another important chemical property of carbon nanotubes. Due to the high gas adsorption capacity of CNTs, it is possible to use them to store hydrogen for hydrogen fuel cells [80]. Furthermore, significant electronic response of nanotubes to chemical adsorption can be obtained, giving rise to applications as chemical sensors [81]. Combined with nano-scale dimension, the unique electrochemical properties will also greatly stimulate applications in the fabrication of electrodes of lithium batteries [82] and electrochemical supercapacitors [83].

2.2 Synthesis of carbon nanotubes

Carbon nanotubes have been synthesized mainly by three techniques: arc discharge, laser ablation, and chemical vapor deposition (CVD). Among them, CVD has been the most widely investigated for synthesizing carbon nanotubes due to its large-scale production ability and high growth controllability. In this section, arc discharge, laser ablation, and CVD techniques will all be introduced with the emphasis mostly on CVD techniques.

2.2.1 Arc discharge and laser ablation synthesis of carbon nanotubes

Arc discharge method has been widely used for producing C_{60} fullerenes. In 1991, Iijima [41] reported the production of MWCNTs by this method for the first time. Later, SWC-

NTs were also successfully produced by Iijima and his colleagues using the same method [84]. Schematic of an arc discharge chamber is shown in Fig. 2.1 [85]. Two graphite rods are placed end to end with a distance of about 1mm, acting as two separated electrodes. The chamber is usually filled with low pressure noble gas. When a voltage is applied, a direct current will be produced and create a high temperature discharge between the two electrodes. The high energy discharge will vaporize one graphite electrode and form carbon nanotubes on another one. Tube diameter has been found to have a close relationship with the composition in gas mixture, the temperature, and the metal catalyst density. High yield of carbon nanotubes can be obtained with uniform plasma arc and high temperature. Although this technique is easy to be operated, the resulted product contains many impurities including amorphous carbon, fullerenes and graphite particles. In laser ablation method, laser is used to vaporize a graphite target in an oven that is filled with helium or argon gas at a pressure of approximately 500 Torr (Fig. 2.1) and an extremely hot vapor plume forms on the target surface and will vaporize carbon target, which sometimes is coupled with metal catalyst, to form carbon nanotubes on the counter collector. Smalley *et al*. [86] are the first in reporting production of carbon nanotubes by laser ablation. But just like arc discharge synthesis, many by-products are formed together with nanotubes.

2.2.2 Chemical vapor deposition of carbon nanotubes

Chemical vapor deposition (CVD) synthesis usually involves the decomposition of hydrocarbons over catalyst, thus it is also called catalytic chemical vapor deposition (CCVD). CVD was firstly used to produce carbon nanotubes by Yacaman *et al.* in 1993 [87]. Then in 1994, Ivanov *et al*. [88] and Amelinckx *et al.* [89] reported the successful synthesis of carbon nanotubes using the same method. Since then, many works have been done in improving and optimizing CVD techniques to carry out large-scale controllable growth of carbon nanotubes [90]. In principle, CVD synthesis of CNTs is a process involving decomposition of carbon containing gases into reactive atomic carbon by different energy sources, diffusion of the carbon towards substrate and into particles of catalyst (typically Fe, Ni, or Co), and finally the precipitation of carbon to form carbon nanotubes. Tube diameter, growth rate, orientation and position can be controlled by adjustment of CVD

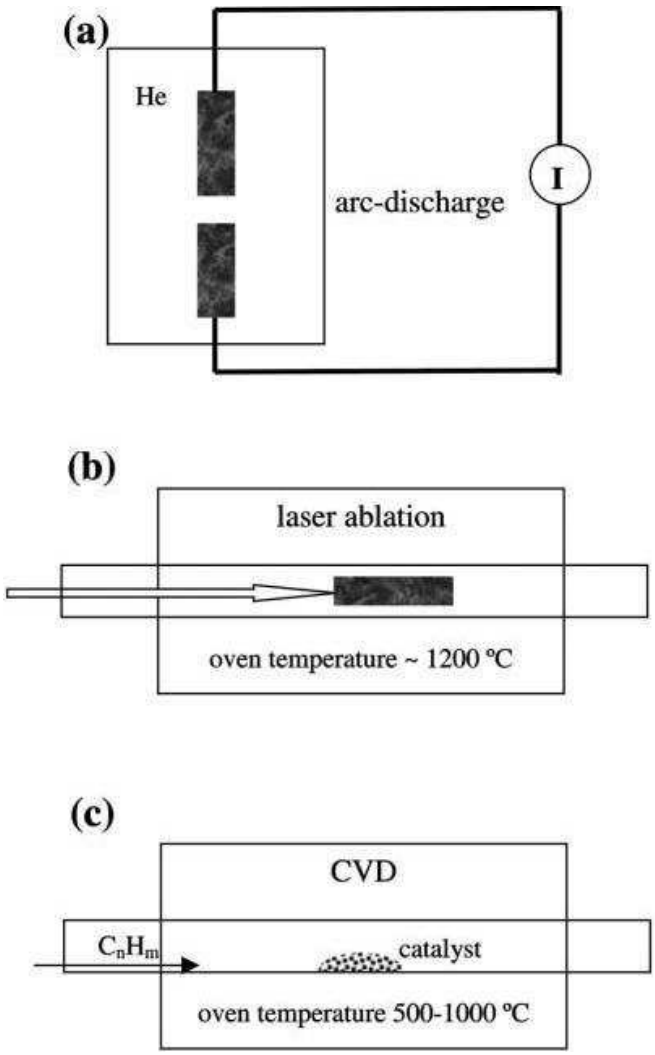

Figure 2.1: Schematic of setups for nanotube growth methods [85].

conditions. The concentration and types of carbon sources, catalysts, and growth temperature are the three key parameters in nanotube CVD growth [85]. Depending on the form of energy to break down hydrocarbons, there are three CVD techniques widely used for nanotube growth: thermal CVD, hot filament CVD (HFCVD), and plasma enhanced CVD (PECVD). These techniques are introduced respectively in the following sections. General CVD growth mechanism is also introduced.

Thermal CVD

In thermal CVD (TCVD), heat is the only energy source to decompose the carbon source and the temperature is usually uniform in the whole reaction chamber. The apparatus

for TCVD are usually composed of a quartz tube, a furnace and a gas line, as shown in Fig. 2.1. Catalyst is introduced into the system by either supported catalyst [91] or floating catalyst [92]. For supported catalyst, catalyst is deposited onto substrate, whereas for floating catalyst, the catalyst particles are formed in-situ from gas. TCVD has been used to grow CNTs since 1993 due to its low equipment cost and simple process. Both MWCNTs [93] and SWCNTs [91, 92] have been synthesized by TCVD. Nevertheless, TCVD requires higher growth temperature than the other two CVD techniques. Especially, SWCNTs can only be synthesized when the temperature is over 900°C and the catalyst particle size is small [94].

HFCVD

Hot filament CVD utilizes tungsten filament(s) which is(are) hung over the substrate holder within a given distance and electrically heated to around 2000°C [37]. The heated filament will decompose gas source and heat the substrate. Same as TCVD, either supported catalyst on substrate [37] or floating catalyst in vapor phase [95] is required for growth of CNTs using HFVCD. Ferrocene has been widely used as floating catalyst source for continuous production of both MWCNTs and SWCNTs [95] whereas coated catalyst patterns have been widely used for controlled pattern growth of CNTs [37]. One of the advantages of HFCVD over TCVD is that it can significantly lower the substrate temperature due to higher filament temperature. For example, the required temperature for nanotube growth is between 900 and 1100°C [96] by TCVD and can be lowered to 750 - 850°C [97] when using HF-CVD. In addition, HFCVD is very versatile and easy to be modified according to research needs, which is necessary for controlled growth of carbon nanotubes.

PECVD

In Plasma enhanced CVD, different from thermal CVD, molecules are activated by a nonequilibrium plasma. A variety of plasma sources have been attempted for PECVD nanotube growth, including direct current (DC PECVD) [23,98], magnetron type radio frequency (rf PECVD) [99], inductively coupled plasma (ICP PECVD) [100], microwave(M-

PECVD) [10, 21, 101–103], electron cyclotron resonance (ECR PECVD) [104], and a combination of HFCVD and DC plasma (HF-DC PECVD) [27, 105]. To understand basic processes that happen in plasmas, a simple example of DC PECVD is given here. Low pressure gas mixture fills the space between two electrodes and a glow discharge is initiated by applying a DC voltage. Four regions of the glow discharge across from cathode to anode are cathode dark space, negative glow, faraday dark space, and positive column [23]. The ions are driven by the applied voltage to bombard the substrate and generate secondary electrons. The secondary electrons are repelled away from substrate (cathode) and ionize some of the excited molecules. These processes are indispensable in sustaining DC discharge. And the excitation process results in negative glow. By plasma assistance, the activation energy can be significantly reduced, leading to decreased growth temperature. Recently, PECVD nanotube growths at as low as room temperature have been reported [106]. These results are very inspiring since low substrate temperature growth is in highly demanding in many applications. For example, growth temperature lower than the soda lime glass substrate melting temperature of 500°C is required in applications of carbon nanotubes as field emission display [27]. In addition, PECVD can facilitate the growth of well dispersed aligned carbon nanotubes. In contrast, only densely packed alignment resulted from crowd effect can be observed using the other two CVD processes, in which the dense compacting is harmful to the field emission properties of nanotubes [107].

2.2.3 Growth mechanism of CNT growth in CVD

To grow CNTs by CVD requires catalyst either pre-coated on the substrate or in vapor phase. And the catalytic nanoparticles are required for CNT growth rather than smooth catalyst layer. CVD growing CNTs, in general speaking, will experience five steps in sequence [90]: 1) precursor(s) diffuse through a thin boundary layer to the substrate. 2) These reactive species are adsorbed onto the particle surface. 3) Surface reactions take place to produce nanotubes and by products. 4) Gaseous byproducts are desorbed from the surface. 5) Outgassing species diffuse through the boundary layer into the bulk stream. One or more of these steps may be rate controlling, varying from case to case. Two

growth models have been proposed to explain the growth of CNT by CVD: surface carbon diffusion [108] and bulk carbon diffusion [109]. Surface carbon diffusion mechanism is commonly used to explain low temperature growth especially with Ni catalyst. Carbon species dissociate and diffuse around the surface and carbon nanotube nucleates on the side of the metal particles. Subsequently the tube continues to grow when carbon continually breaks down on the particle. In bulk carbon diffusion model, the carbon feedstock breaks down on the surface of the metal particle and the carbon dissolves into metal particles. The dissolution proceeds on until the saturation point is reached. At this point, the CNTs start to grow from the outer surface and two sub-models are proposed to describe the CNT growth after this point. If the catalyst particles adhere tightly to the substrate surface, CNTs grow out from the top surface of the catalyst particles leaving the particles on the substrate surface. In contrast, the weak adhesion of particles to the substrate results in the lift up of particles from the substrate surface by the growing CNTs, in which, catalyst particle can be observed at the top end of tubes. The first scenario is called base growth whereas the second one is called tip growth. Figure 2.2 displays these two CNT growth models.

2.3 Direct growth of carbon nanotubes in CVD

CVD have been widely used in synthesizing carbon nanotubes, owing to its distinct advantages over other techniques such as laser ablation and arc discharge. These advantages include the lower growth temperature and the flexibility to produce well-aligned CNT arrays for field electron emission applications [110, 111]. Nevertheless, CVD approach needs assistance of catalysts, generally being transition metal nanoparticles, for efficient CNT growth. Additionally, non-metal materials have often been pre-coated onto metal substrates to reduce the catalyst-metal interaction. These requirements greatly limit the application of CNT in field emission devices. For example, the non-metal interlayer between the metals and CNTs may result in unstable emission current [2] and thus post-processing is required to remove the interlayer. Even worse, the removal process raises the risk of losing CNTs and their desired properties. In this regard, it is essentially important to find

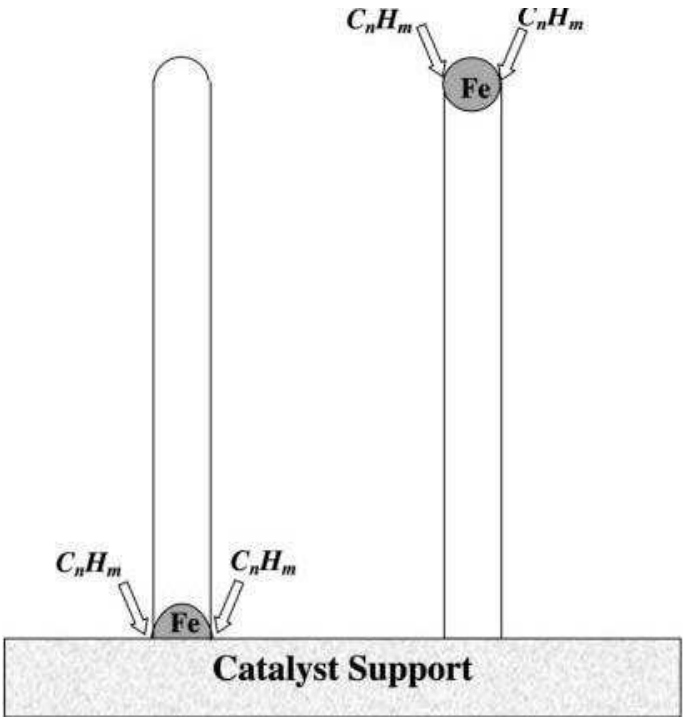

Figure 2.2: General growth modes of nanotube in chemical vapor deposition. Left represents the base growth mode and right represents the tip growth mode [85].

ways to grow aligned CNT arrays directly on metals without any additional catalyst [112].

A number of works have been done on using oxidation-reduction method to generate catalyst particles in-situ from a variety of metal substrates to grow CNTs directly on the substrates [3, 5, 6]. Yang *et al.* [111] have synthesized large-quantity of carbon nanotubes directly on stainless steel using thermal CVD to decompose ethanol. Soneda and Makino [113] obtained CNTs by thermal decomposition of CO over stainless steel. Both results indicate that catalyst particles can be generated from metal substrate through thermal pre-treatment. However, it is difficult to control the morphologies of the resulted CNTs. Plasma has been proved to be effective in breaking catalyst layers and producing catalyst particles. Hirakawa *et al.* have grown carbon nanotubes directly on SUS304, nickel, Inconel-600, and Invar-42 substrates using PECVD [9]. Park *et al.* [4] adopted an innovative way to synthesize CNTs directly on stainless steel plates: a sequential combination of PECVD and thermal CVD. PECVD is supposed to nucleate and initiate the CNT growth while thermal CVD is used for further growth. Bias enhanced microwave

plasma chemical vapor deposition technique was also utilized in direct synthesis of CNTs. Using this technique, carbon nanotubes were grown directly on a Fe, Ni, 304 stainless steel [2, 7] and Fe-Ni-Cr alloy [8] respectively. In those two studies, a negative bias was applied to substrate in a plasma, and the substrates were etched in the hydrogen plasma for 30 min before the growth [2, 8], which was believed to enhance the formation of catalytic sites for CNT nucleation. Without hydrogen plasma pre-etching, CNTs were also obtained on stainless steel [7], indicating that CNT nucleation can be initiated under CNT growth conditions in a plasma. Particularly, Yang *et al*. [10] have successfully synthesized carbon nanotubes on inconel-600 plates at temperature lower than 550°C in a bias enhanced MPECVD system. Plasma aided Hot Filament CVD [29] was also used to directly grow CNTs on single crystalline Ni wafers and the synthesis was carried out in two steps: high bias voltage was applied for CNT nucleation, and lowered bias voltage was applied for CNT growth.

Oxidation-reduction process on a metal substrate is one of the main methods to produce catalysts in-situ from the substrate. Oxidation immobilizes the catalyst and prevents clustering, whereas reduction activates the catalyst through conversion of oxides into elemental metal state. Vander Wal and Hall [5] have used thermal oxidation and laser oxidation to pre-treat stainless steel mesh, followed by in-situ reduction. CNTs were successfully grown on the mesh in both cases. Karwa *et al*. [6] reported similar results regarding direct growth of CNTs on stainless steel in which the oxidation, reduction, and growth were proceeded sequently in a thermal CVD chamber, and the effects of flow rate and deposition time on the length of CNTs were studied. The quality of the nanotubes formed was found to be influenced by the oxidation temperature. However, the effect of the pretreatment temperature on the formation of oxides and thus the quality of the resulted CNTs was not investigated. In this thesis, the direct synthesis of CNTs on Inconel sheets pre-treated in air at different temperatures by using plasma enhanced hot filament CVD (HFCVD) and the FEE properties of the resulted CNTs are being investigated in order to optimize the growth conditions to obtain CNTs with superior FEE properties.

2.4 Aligned growth of carbon nanotubes by CVD

Due to the unique electrical, chemical, and mechanical properties, as well as the high aspect ratios and small radius of curvature at their tips, carbon nanotubes are of great potential in many applications. Being a functional ensemble, they are utilized in such applications as catalyst supports, supercapacitors, and fuel cells electrodes [114]; being single nanotube, they are used individually as functional components in devices such as field emitters [115], electron sources [116], transistors [54], and scanning probe tips [117]. For many of the aforementioned applications, it is desirable to fabricate carbon nanotubes with controlled alignment and orientation. Vertically aligned carbon nanotubes are of great interests in applications such as electron-field emitters in panel display, scanning probe microscope tips, biological probes, and interconnect for nanoelectronics. To date, aligned growth of nanotubes using both thermal CVD and plasma enhanced CVD have been reported and different alignment mechanisms have been proposed.

2.4.1 Aligned growth by TCVD

Two methods are usually adopted in TCVD growth of aligned carbon nanotubes. One is to pre-deposit densely arranged catalyst particles onto the substrate. The crowding effect will then force the growing carbon nanotubes to be aligned. Fan *et al*. [20] used porous silicon as substrates and deposited catalyst by electron beam evaporation in which shadow masks have been used for patterning. After deposition, aligned growth was observed within each block with high density of carbon nanotubes attracted to each other by van der Waals force. The other way is to template CVD by which nanotubes were grown within highly ordered pores on template membrane placed on the substrate [118]. The alignment in this case was attributed to the constraint imposed by the pores as well as Van der Waals interaction in between. Anodic aluminum oxide (AAO) is one of the most commonly used template materials that have nanopores patterned in a hexagonal order. Catalyst is then filled into pores by electrochemical deposition, or electroless deposition. After nanotube deposition, the template can be etched away. The synthesis of aligned CNTs by template method was first reported in 1995 [18]. Martin [19] and his group have been devoted in this technique

for years to grow aligned carbon nanotubes with small diameters of about 20 nm.

2.4.2 Aligned growth by PECVD

Due to its versatility and flexibility, PECVD has attracted great interests in synthesizing aligned carbon nanotubes. A few alignment mechanisms have also been proposed to explain the growth results in different plasma apparatus under different plasma conditions.

Zhang *et al*. [22] applied a DC and an ac voltage respectively to a quartz supported polycrystalline silicon film to synthesize CNTs by CVD process. Prior to CVD process, tree parallel trenches were formed on the silicon film by plasma etching. After then, catalyst was transferred onto the substrate film by contact printing. During the CVD deposition, methane and hydrogen were used as gas sources. After CVD deposition, SWCNTs were observed suspending across over the trenches. Although no plasma was generated, it was proposed that the electric field was the origin of the alignment of CNTs and polarization induced alignment was the key mechanism, in which large aligning torques and forces originated from dipole moments are the keys in the alignment of nanotubes.

Similar to Zhang's experiment, Avigal and Kalish [119] utilized a DC voltage for aligning nanotubes. But in their experiment, substrate is one of the electrodes with the counter electrode placing above it, thus producing a plasma in the space between the two electrodes. The results show that negative bias on the substrate facilitated vertically aligned CNTs, whereas positive bias resulted in randomly oriented CNTs. The alignment was proposed to be associated with Coulomb attraction. A DC PECVD process was also used by Chen *et al*. [120] to grow arrays of aligned CNTs. Nanotube morphology was found to have strong dependence on electric field. By increasing the bias voltage, the transition from nanotube to nanocone structure occurred. Plasma etching was reported to be the transition mechanism. Chhowalla *et al*. [98] also reported vertically aligned CNT growth by a DC PECVD process. They investigated the effect of different growth parameters, including catalyst layer thickness, bias voltage, deposition temperature, gas composition, and pressure on the growth and alignment of CNTs and concluded that the alignment of CNTs was due to the effect of electric field.

Merkulov *et al.* [23–25] synthesized vertically aligned carbon nanofibers (CNFs) by

DC PECVD. In their experiment, a glow discharge was initiated around the substrate and a negative bias voltage of 550V and a current of 100mA were applied. The result show that both aligned and non-aligned CNFs were grown on the substrate in a single growth process, in which catalyst particles were found on the aligned CNFs and not on the non-aligned ones. Based on this observation, a CNT aligning model was proposed, as shown in Fig. 2.3. In the case of tip growth, electrostatic force causes a compressive force at the particle/nanofiber interface where growth rate is higher, and a tensile force at the interface spot where growth rate is lower. The resultant net force is in favor of balance the growth rate around the entire periphery thus stabilizing the aligned growth, and the orientation of CNFs is along the applied electric field line direction. In contrast, compressive force is produced at lower growth rate spot while tensile stress is localized at higher growth rate spot in the case of base growth. As a result, the stress feedback will further misalign CNFs, thus resulting in randomly oriented CNTs.

Microwave plasma enhanced chemical vapor deposition (MPECVD) is one of the most commonly used techniques to grow aligned CNTs. Bower *et al*. [21, 26] reported CNT growth using MPECVD and the result show that the tube axes are always perpendicular to the local substrate surface regardless of the substrate shapes or tilt angles. It was suggested that CNTs were aligned by the electric field produced by the self-bias potential imposed on substrate surface. The electric field is always perpendicular to the substrate surface regardless of the substrate shape or tilt angles. However, Chen *et al*. [33] thought that the self-bias is not high enough to align the CNT. In their reports, random oriented spaghetti like morphology was obtained using CH_4 / H_2 mixture in a MPECVD system, but N_2 addition leaded to the vertical alignment of CNTs. They attributed the alignment to crowding effect. Tsai *et al*. [101] have proposed another CNT growth mechanism in MPECVD, in which anisotropic etching is responsible for alignment growth. It is reported that ion etching removes nanotubes that are unparallel to the ion movement direction. However, this mechanism can not explain the coexistence of random and aligned CNTs in a single growth process. Apart from alignment mechanism investigation, many other works have been focused on how to control the growth of aligned CNTs [33].

Plasma enhanced hot filament chemical vapor deposition (PE-HF-CVD) has also been

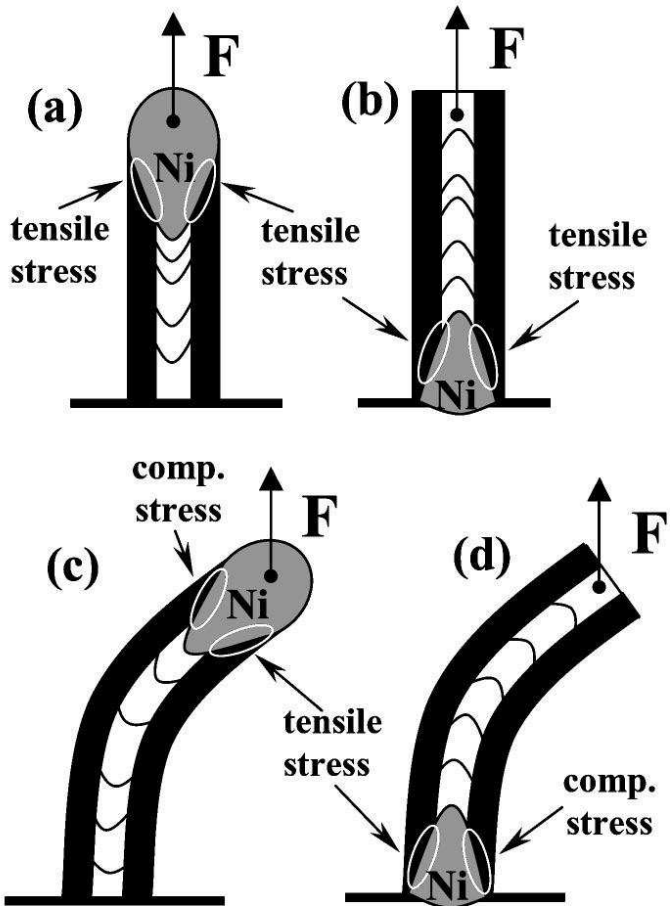

Figure 2.3: Schematic diagrams of alignment mechanism [24].

proved to be an effective technique to grow aligned CNTs. A DC bias is usually added to the filament and substrate holder to produce a plasma between them. Ren *et al.* [27, 28] have reported that large area of well-aligned CNTs can be synthesized on glass by PE-HFCVD. Plasma intensity was found critical in determining nanotube aspect ratio and height distribution, which in turn affect the field emission properties of the aligned CNTs. But the alignment mechanism was not given. Chen *et al*. [29,30] also used DC PE-HFCVD to grow aligned CNTs and found that nanotube orientation can be controlled by tilt the substrate during growth and the alignment mechanism were attributed to the electric field. Other works regarding the effect of growth parameters on the aligned growth of CNTs have also been reported. Huang *et al*. [121] reported the effect of catalyst on the aligned growth of CNTs. Nickel, iron and cobalt were used respectively as catalyst using PE-HFCVD. It was shown that nickel resulted in the biggest nanotube diameter and thus was

the best catalyst to obtain aligned CNTs.

In this thesis, co-growth of random and aligned CNTs has been observed in the early stage using DC PE-HFCVD, which can not be explained by Chen's mechanism. In order to achieve controlled growth of CNTs, it is essential to fully understand the alignment mechanism. In this thesis, a wide range of bias voltage was applied during CNT growth, and the structural evolution of the resulted CNTs was monitored for mechanism speculation. In addition, the effect of substrate pre-scratching on alignment was also investigated.

2.5 Secondary growth of carbon nanotubes by CVD

Recently, the secondary growth of carbon nanotubes on primary carbon nanotubes has attracted growing interests for catalysis and sensor applications [14]. It has been found that the growth of secondary CNTs can enlarge the surface area remarkably [122]. An enhanced amperometric sensing for glucose has been reported through the growth of secondary CNTs in a multiple- branching manner [13]. The secondary CNTs were investigated to enhance field electron emission, showing great potential in improving uniformity and efficiency of field emission flat panel displays [17, 123].

A number of works have been done in growing secondary CNTs [13–15, 17]. The results show that catalyst layers are necessary in order to grow CNTs with different structure on the primary CNTs. To simplify the secondary growth process, it is in demanding to obtain secondary CNTs directly on primary CNTs without addition of any catalysts. In this thesis, very low carbon concentration has been used to grow primary CNTs, and followed by secondary CNTs growth by simply increasing carbon source concentration. No catalyst deposition was needed throughout the whole process. The mechanism for the secondary CNT growth and the FEE properties of resulted CNTs have also been investigated have also been investigated. Significant improvement of field emission properties has been observed.

2.6 Field electron emission

2.6.1 Field electron emission theories

Free flowing electrons are widely used in many areas including electron microscopy, Cathode Ray Tube (CRT) display, X-ray generation, electron-beam lithography, surface treatment and thin film deposition [124]. Free electrons can be generated through two ways in high vacuum environment. One is using external energy source to energize electrons and make them escape the potential barrier at the solid surface. The most common technique used is thermionic emission, in which thermal energy is applied to provide sufficient kinetic energy for electrons to overcome the surface potential barrier. The main drawbacks of thermionic emission are low efficiency caused by energy loss in radiation, filament deformation, and finite lifespan of the filament. An alternative choice is to reduce or thin the barrier for electrons to tunnel through. High electric field is well-proven to be competent and to induce electron emission. Normally an extremely high electric field (several $kV/\mu m$) is in need. In practical cases, local field enhancement is the only solution for such a high–field demand. Thus, a conducting sharp tip structure is usually used as a field emission cathode, which can reduce macroscopic start-on electric field to just a few $V/\mu m$. The conducting nature, nanoscale dimension, and sharp tip end all make CNTs ideal as field electron emitters.

The Fowler-Nordheim (FN) theory is used to analyze field emission from CNTs. A FN equation is presented as follows:

$$I = AJ = At_N^{-2} a\phi^{-1}\beta^2 E^2 \exp\left[-\upsilon_N b\phi^{3/2}/(\beta E)\right], \tag{2.1}$$

where I is the emission current and J is the emission current density (here, J is taken as a constant over a notional emission area A). ϕ is the local work function, $E = V/d$ is the macroscopic electric field (i.e., E is the electric field in a parallel-plate configuration and is defined by the ratio of applied voltage V to the probe-sample distance d) and β is the field enhancement factor (FEF) that relates to the field F in the tunneling barrier to E (i.e. $F = \beta E$). The quantities $a(= 1.5410^{-6} AeVV^{-2})$ and $b(= 6.8310^{9} eV^{-3/2}Vm^{-1})$ are universal constants, and υ_N and t_N are called Nordheim functions. Details of derivation

can be found in [125, 126]. A field emission test result can be plotted in $ln(I/E^2)$ versus $(1/E)$ coordinates and the working equation for FN plot is

$$\ln(I/E^2) = \ln(\alpha a \phi^{-1} \beta^2) - b\phi^{3/2}/(\beta E), \tag{2.2}$$

More details can be found in [127]. In this equation, α is called "effective emission area".

2.6.2 Field emission performances of CNTs films

Many factors have been reported to have impacts on the field emission characteristics of CNTs. One of the primary factors is the screening effect. It is a situation in which nanotubes are too close to each other so that one CNT tip can be shielded from the macroscopic electric field by other CNTs, resulting in impaired emission property. Hence, density control over CNT films has great significance in CNT field emitter design. Nilsson *et al*. [128] predicted that optimum field emission occurs when the tube height is about one half of the intertube spaces. AAO template method was used by Suh *et al*. [107] to grow highly ordered CNT arrays and the best emission result was observed when intertube distance equals to the tube height. Screen effect has also been observed for a variety of CNT morphologies. CNT bundles of different density showed different emission characteristics [129]. Short and stubby aligned CNTs are better field emitter than those with higher aspect ratios [130].

Orientation of CNTs is another important decisive factor affecting emission properties. The CNTs deviated from the substrate normal performed better in field emission than vertically aligned ones did [30], because more emission sites (e.g., defects) are on the sidewalls of CNTs. Additionally, factors such as the state of tube ends [2] and surface treatment on CNTs [131] can also largely influence the field emission properties of CNTs.

CHAPTER 3

MATERIALS AND EXPERIMENTAL METHODS

3.1 Substrate material and pre-treatment

The substrate alloy used in this thesis was Inconel 600 alloy (a nickel–based superalloy). Its chemical composition is shown in Table 3.1.

Although nanoparticles of Ni, Fe or Co or their alloys are widely used as catalysts for CVD growth of CNTs, successful synthesis of CNTs directly on Inconel 600 substrate without the addition of any catalyst was only reported by Hirakawa *et al*., using plasma-enhanced CVD in a methane and hydrogen gas mixture [9]. Synthesis of CNTs on Inconel 600 substrate was also reported by Talapatra *et al*. using floating catalyst CVD [11]. Yang *et al*. recently reported that randomly distributed CNTs can be feasibly grown on Inconel 600 plates at low temperatures using microwave plasma enhanced CVD [10]. In this thesis, the CNTs were synthesized on Inconel plates without any additional catalysts by hot filament CVD (HFCVD). Pre-oxidation were employed in order to produce catalyst particles on substrate surface. The pre-treatment were conducted using a muffle furnace. The gas atmosphere was air. The furnace was heated to the pre-set temperature (800°C, 900°C, 1000°C, and 1100°C, respectively) first, and then kept at the temperature for 3 hours for stabilization. The Inconel sheets (10 mm $\times$ 10 mm $\times$ 0.3 mm) were then placed on a firebrick and put into the furnace. After 1 h, the electrical power of the furnace was shut down and the treated sheets were cooled down within the furnace.

Table 3.1: Composition of Inconel 600 alloy.

Element	Ni	Cr	Cu	Fe	Mn	Si	S	P	C
wt.%	72.0	15.5	0.5	8.0	1.0	0.5	0.015	0.015	0.065

3.2 Hot filament chemical vapor deposition reactor

The schematic diagram of the hot filament CVD (HFCVD) reactor used in the present work is shown in Figure 3.1. The HFCVD reactor (image shown in Figure 3.2) is composed of a vacuum chamber, a gas supply, a pumping system, and an electrical system. The vacuum chamber is a cross–shaped glass tube with a diameter of 15 cm. A diffusion pump combined with a rotary pump makes up the vacuum system. The gas composition and the pressure in the chamber were controlled by a two-channel gas flow controller and a needle valve in the pumping line. The gas mixture was guided by a stainless steel tube directly to the top of the filament in the reaction chamber. The filament in the CVD reactor is a coiled tungsten of ten coils. The coils measured 4 mm in diameter and 4 cm in length. The tungsten wire used to make the coils was 0.3 mm in diameter. The coiled tungsten filament was connected to an AC power source and was Ohmically heated to provide the thermal energy for dissociating the processing gases. An optical pyrometer was used to measure the filament temperature during the CNT deposition. A cooling fan stood by the chamber to dissipate the heat produced by the filament during the growth. A thermocouple was attached to the substrate holder for substrate temperature measurement. According to experimental needs, a DC bias voltage could be applied between the filament and the substrate holder to create a glow discharge or to bias the substrate without starting a discharge.

3.3 Growth of Carbon Nanotubes

The CNT growth was carried out using an HFCVD system, as described in section 3.2. 10 mm $\times$ 10 mm $\times$ 0.3 mm sized Inconel 600 sheets were used as substrates. In some experiments, the substrates were scratched using sand paper prior to the other treatments. Before

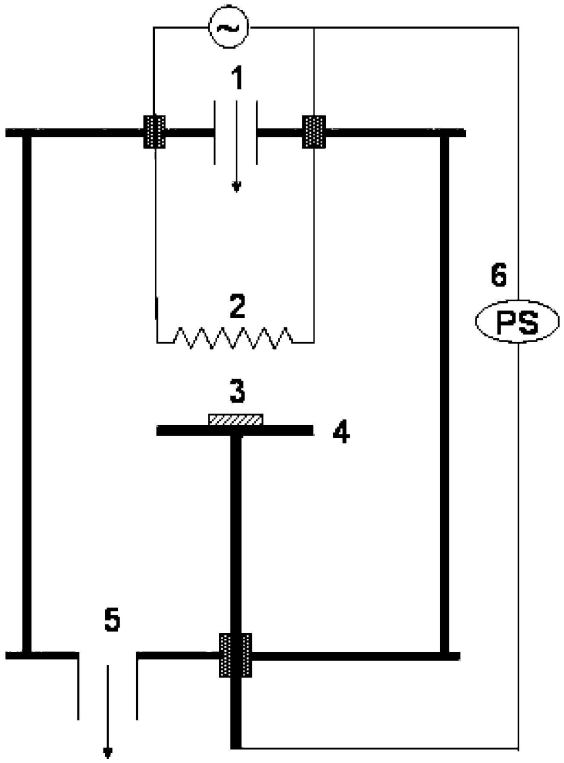

Figure 3.1: Schematic diagram of the hot filament chemical vapor deposition reactor [105].(1: gas inlet, 2: filament, 3: substrate, 4: substrate holder, 5: pump port; 6: dc power supply)

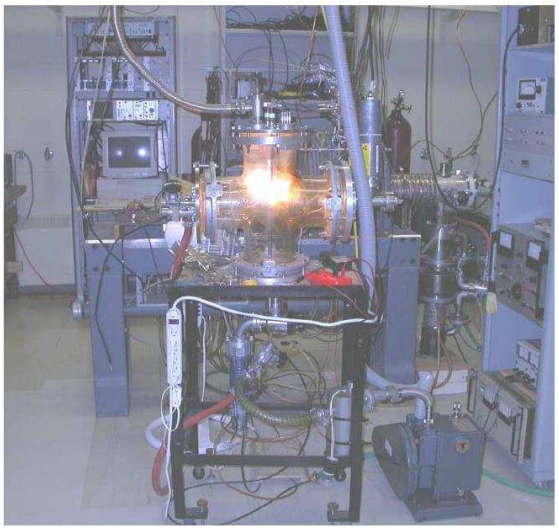

Figure 3.2: A picture of the hot filament chemical vapor deposition reactor.

the CNT growth experiments, the Inconel sheets were heated in air to obtain an oxidized layer on their surfaces as described in section 3.1 and cleaned using ethanol. After the sheets were placed on the substrate holder, the chamber was pumped down to a pressure of 2.7 Pa using a rotary pump and a diffusion pump. Then methane (CH_4) and hydrogen (H_2) gases were introduced through separate mass flow controllers. When the working pressure was stabilized at the preset value of 2.66 kPa, the power supply for filament was turned on. The coiled tungsten filament was heated by an AC power supply at a voltage of 30 V and a current of 9 A. A DC bias voltage was applied between the substrate holder and the filament for aligned growth. The substrate temperature was measured with a thermocouple attached to the backside of the substrate holder. The pre-treatment conditions and growth parameters were varied for different investigation purposes, as listed in Table 3.2.

3.4 Scanning Electron Microscopy

As one of the most widely used surface characterization techniques, scanning electron microscope (SEM) uses a high energy electron beam to scan and image the sample surface. Through interactions between incident electrons and the solid sample atoms, a number of signals are generated and collected, including secondary electrons, back scattered electrons, characteristic X-rays, and light (cathodoluminescence). More details can be found in [132]. Specialized detectors are required for detecting different types of signals. One single SEM machine usually is not assembled with all the detectors. Secondary electron imaging (SEI) is the most commonly used detection mode in the SEM to determine surface morphology because the secondary electron emission is strongly dependent on the incident angle between the probe beam (incident electron beam) and the local surface morphology. The resolution of a SEM is affected by the diameter of the electron probe. Typical resolution for a 20 kV SEM is about 3 nm, much higher than optical microscopes. While secondary electrons are ejected from inelastic scattering interactions between the specimen atoms and incident electrons, backscattering electrons (BSE) are the elastic scattering electrons. BSE are often used to map the elemental distribution in the sample based

Table 3.2: Pre-treatment conditions of substrate sheets and growth parameters of CNTs.

Sample Number	Pre-scratching	Pre-oxidation Temperature (°C)	Bias Voltage (V)	Substrate Temperature (°C)	H_2 Flow Rate (sccm)	CH_4 Flow Rate (sccm)	CH_4 Concentration ($vol.\%$)	Growth Time (h)
1	No	No	-500	620	35	1.8	5	1
2	No	800	-500	620	35	1.8	5	1
3	No	900	-500	620	35	1.8	5	1
4	No	1000	-500	620	35	1.8	5	1
5	No	1100	-500	620	35	1.8	5	1
6	No	1100	0	560	35	0.1	0.28	1/6
7	No	1100	0	560	35	0.1	0.28	1/2
8	No	1100	0	560	35	0.1	0.28	1
9	No	1100	0	560	35	0.1 1.8	0.28 5	1 1/2
10	No	1100	0	560	35	1.8	5	1/6
11	No	1100	0	560	35	1.8	5	1
12	No	1100	0	560	35	1.8	5	1.5
13	No	1100	0	560	35	1.8	5	1
14	No	1100	-400	620	35	1.8	5	1
15	No	1100	-450	620	35	1.8	5	1
16	No	1100	-500	620	35	1.8	5	1
17	No	1100	-500	620	35	1.8	5	1/6
18	No	1100	-500	620	35	1.8	5	1/2
19	No	1100	-550	620	35	1.8	5	1
20	No	1100	+150	620	35	1.8	5	1
21	Yes	1100	-500	620	35	1.8	5	1/6
22	Yes	1100	-500	620	35	1.8	5	1

on the fact that heavier atoms elastically scatter more electrons thus producing brighter images. X-rays can also be detected by a SEM coupled with an energy-dispersive X-ray spectroscopy (EDS) or a wavelength-dispersive X-ray spectroscopy (WDS) equipment. With EDS, it is possible to use SEM to obtain chemical composition information locally and semi quantitatively.

In this thesis, a JEOL JSM 840A SEM operating at 20 KV was used to observe the morphologies of the synthesized CNTs. BSE detection mode was used to identify the position (tip or bottom of CNTs) of catalyst particles. Although limited by its resolution, when combined with other techniques, SEM is still able to analyze the impurities existing in SWCNT bundles [33].

3.5 Transmission Electron Microscopy

Transmission electron microscope (TEM) uses the electron beam as illumination source just like SEM, it has totally different operation principles. SEM utilizes medium- to low-energy focused electron beam probe, ranging from 500 V to 50 kV , to scan over the sample surface. In contrast, TEM uses a high-energy parallel electron beam (100 kV to 200 MV) to transmit through a thin sample foil [133]. The detector is placed on the other side of sample to collect transmitted electrons. Due to the different ways of producing images, a TEM has much higher spatial resolution than a SEM. Another electron microscope is called scanning transmission electron microscope (STEM). In STEM, a high-energy electron beam is used to scan samples and transmitted electrons are collected and analyzed. By integrating the advantages of both SEM and TEM, a STEM can be used to detect sample topology, while possessing an excellent spatial resolution. Diffracted electrons can also be detected in TEM to obtain diffraction patterns of materials locally. By analyzing the positions of the diffraction spots and the image symmetries, information about the space group symmetries in the crystal and the crystal's orientation to the beam path can be obtained. Another advantage of TEM over SEM is that electron energy loss spectrometry (EELS) can also be obtained in a TEM. EELS is a powerful chemical analysis technique that provides users with qualitative and quantitative chemical analysis through measuring

the energy loss of the transmitted electrons.

TEM is a powerful tool to investigate detailed structure of CNTs. Due to its high resolution, it is possible to obtain the number of walls in an MWCNT, to resolve an individual SWCNT within an SWCNT bundle, measure the tube diameter, and investigate defects in CNTs. The electron diffraction and EELS equipped in TEM have also been used to determine the helicity and dopants in CNTs. Coupled with EDS, a TEM can also identify the composition of the catalyst for nanotube nucleation.

However, TEM specimens must be very thin and be able to survive in high vacuum environments. Thus sample preparation for TEM is much more complicated than that for SEM. However, as nanotubes have dimensions small enough to be electron transparent, sample preparation can be easily done by depositing dilute sample that contains nanotubes under analysis onto support grid or films. In this thesis, the synthesized CNTs were firstly scratched off from the substrates and dispersed in 70% alcohol. The solution was vibrated in an ultrasonic device and then deposited onto copper grids. The prepared samples were dried overnight and then analyzed in a Phillips 410LS TEM with an electron energy of 100 KeV.

3.6 X-ray diffraction

X-ray diffractometry (XRD) is a non-destructive technique based on the elastic scattering [132]. Basically, X-ray diffraction is obtained when an X-ray beam is diffracted from planes of atoms in a crystalline material, in accordance with the Bragg's law. Constructive interference results in intensity peaks whereas destructive interference does not. Identification of the phase composition of materials can be achieved by a procedure called indexing of X-ray diffraction data. It is a technique for comparing the diffraction patterns of an unknown sample with standard patterns. Apart from peak positions, peak heights are also useful in XRD analysis. The amounts of the components in a solid material can be estimated by measuring peak heights in an X-ray diffraction pattern. It is also possible to determine crystallinity and particle size of a sample by comparing XRD patterns of the test material with that of the same crystalline material. Another application of the XRD

technique is to measure residual stresses. Residual stresses change the lattice parameters of crystals, and XRD can determine these stresses through the measurement of the lattice parameters. Texture, the preferred orientation of crystallites in a specimen, can also be determined by XRD through investigating the intensity changes of diffraction peaks with the change of the incident angle. By analyzing the width and the shape of the diffraction peaks, crystallite size can also be determined.

XRD is usually used to identify the formation of CNTs [39]. However, XRD alone can not confirm the formation of CNTs. XRD patterns are also used to identify the catalyst materials for CNT growth and distinguish between SWNT and MWNT. [40]. In this thesis, XRD measurements were done using a Rigaku (Rotaflex Ru-200) diffractometer to determine phase changes in the Inconel sheets after pre-treatment and growth. The X-rays used was the Cu Kα line (λ = 0.15418 nm) produced by the impact of an 80 kV, 40 mA electron beam. The collected 2θ range is from 3 to 100°.

3.7 Raman Spectroscopy

Raman effect is basically the inelastic scattering of light by matter [134]. It can be depicted through an energy level diagram. First of all, assume the molecular system has two vibrational energy levels, denoted as n=0 for ground state and n=1 for excited state. If the energy difference of the two states is $h\upsilon_m$ and the incident light has a frequency $h\upsilon_l$, the emitted light will have different different frequencies:υ_L, $\upsilon_L - \upsilon_M$, $\upsilon_L + \upsilon_M$. The emitted light has the same frequency is due to the elastic or Rayleigh scattering. The frequency shifted to $\upsilon_L - \upsilon_M$ and $\upsilon_L + \upsilon_M$ is due to Stokes or anti-Stokes Raman scattering, respectively. At ambient temperatures, Stoke Raman scattering are generally much more intense. Thus, it is usually the Stokes Raman spectrum that has been studied. The frequency distribution of the scattered light dictates the characteristics of the molecular structure or bonding states of the matter that scatters the light. Therefore, Raman spectroscopy is widely used to determine molecular structure or bonding states of materials. Raman spectroscopy is non-destructive and operated in ambient environment, simple and fast. MicroRaman spectrometer can be used to analyze structures locally in a very small

area.

Raman spectroscopy is a very powerful technique for analyzing carbon materials. It can be used to differentiate SWCNTS and MWCNTS, diamond and graphitic structures [37] and to determine the diameter, chirality, dopants, and intercalation properties of SWCNTS [38]. A micro-Raman (Renishaw 2000) system operated at the argon laser wavelength of 514 nm with a spot size of approximately 1 μ m was used in this thesis to analyze CNTs.

3.8 Field Emission Measurement

In field electron emission (FEE) measurements, a very high vacuum is normally required for the sake of accuracy of the measurements. Otherwise, the emitted electrons would be adsorbed by air molecules and the ionization of air molecules would cause avalanche breakdown, resulting in fake FEE current. In this research work, a field electron emission measurement device was designed and set up, as shown in Figure 3.3. The system can reach a base pressure of $(1-2)*10^7$ Torr in 3 hours by a turbo molecular pump combining with a mechanical pump. And high vacuum environment can be maintained during the measurement process. The anode and sample were placed in a stainless steel vacuum chamber. The diameter of the stainless steel anode is 1 mm, and the anode-cathode spacing can be adjusted using a micrometer in the range of $0 \sim 100\ \mu m$. The high voltage power source used for the field electron emission measurement is Keithley 237. The Keithley 237 is an instrument programmed to source and measure voltage and current simultaneously. The Keithley 237 was connected to a PC using IEEE 488 (GPIB) card. Labview software was used to perform the data acquisition. The current – voltage (IE) measurements were performed at room temperature in a high vacuum chamber. And the field electron emission I-E curve and corresponding F-N plot can be obtained and displayed on the computer screen simultaneously. In order to adjust the distance between anode and cathode without damaging the sample surface, the resistance between the anode and sample was monitored when the anode was moved toward the sample. The zero distance point was set where the resistance changes from infinity to a certain value. Then the anode was moved away to the

desired distance for the consequent measurement. To protect sample from large emission current, a limitation of maximum emission current was set prior to each FEE test.

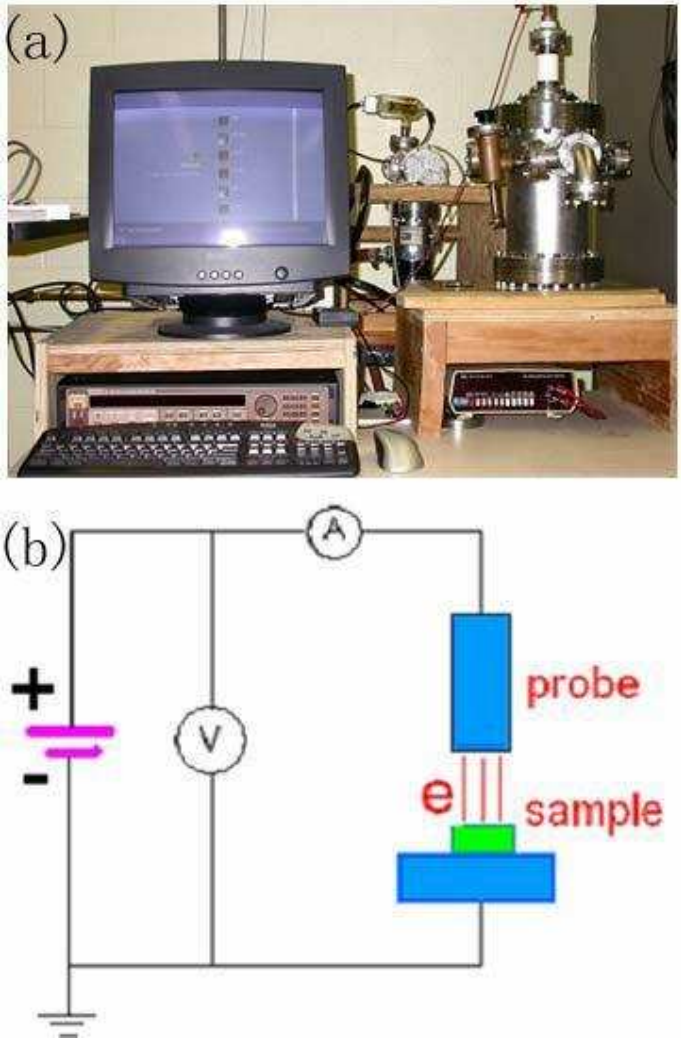

Figure 3.3: Device image (a) and schematics (b) of set-up for field electron emission measurement. The left part of (a) is Keithley 237 unit. The right part of (a) is the high vacuum chamber with the test probe and sample inside [135].

CHAPTER 4

RESULTS AND DISCUSSION

4.1 The effect of pre-treatment temperature on direct growth and field electron emission of aligned carbon nanotubes on Inconel

Figure 4.1 shows SEM micrographs of carbon materials deposited on untreated Inconel substrate (Fig. 4.1a), and 800°C (Fig. 4.1b), 900°C (Fig. 4.1c), 1000°C (Fig. 4.1d), and 1100°C (Fig. 4.1e) pre-oxidized Inconel substrates, respectively. Well aligned ensembles of nanofiber structures were grown on all the pre-treated substrates whereas the structures formed over the untreated substrate were not fiber-like. TEM observation (Fig. 4.2) and Raman spectra (Fig. 4.7) verified that the nanofiber structures grown on the pretreated substrates were CNTs. The result demonstrates clearly that oxidation pre-treatment is efficient in improving CNT growth. From Figure 4.1, we can also see that the CNTs on the 1100°C pre-oxidized substrate exhibit the best alignment (Fig. 4.1e) and there are more crooked and twisted CNTs weaving into bundles as the pre-treatment temperature decreases. The top-view SEM morphologies of the samples are presented in Figure 4.3. It is also interesting that the surface of CNTs grown at 800°C pretreated substarte (Fig. 4.3a) is capped with unevenly distributed and severely agglomerated particles, whereas the caps on the surface of CNTs grown on substrates at higher pre-treatment temperature (Fig. 4.3b - 4.3d) are finer and more uniformly distributed and exhibit better separation with less agglomeration. The particles capped on the top of the CNTs are considered to be peeled off from the substrate and lifted up by the up-growing nanotubes. Fig. 4.3e and 4.3f are the enlarged SEM images of the CNTs samples grown on 800°C and 1100°C pre-

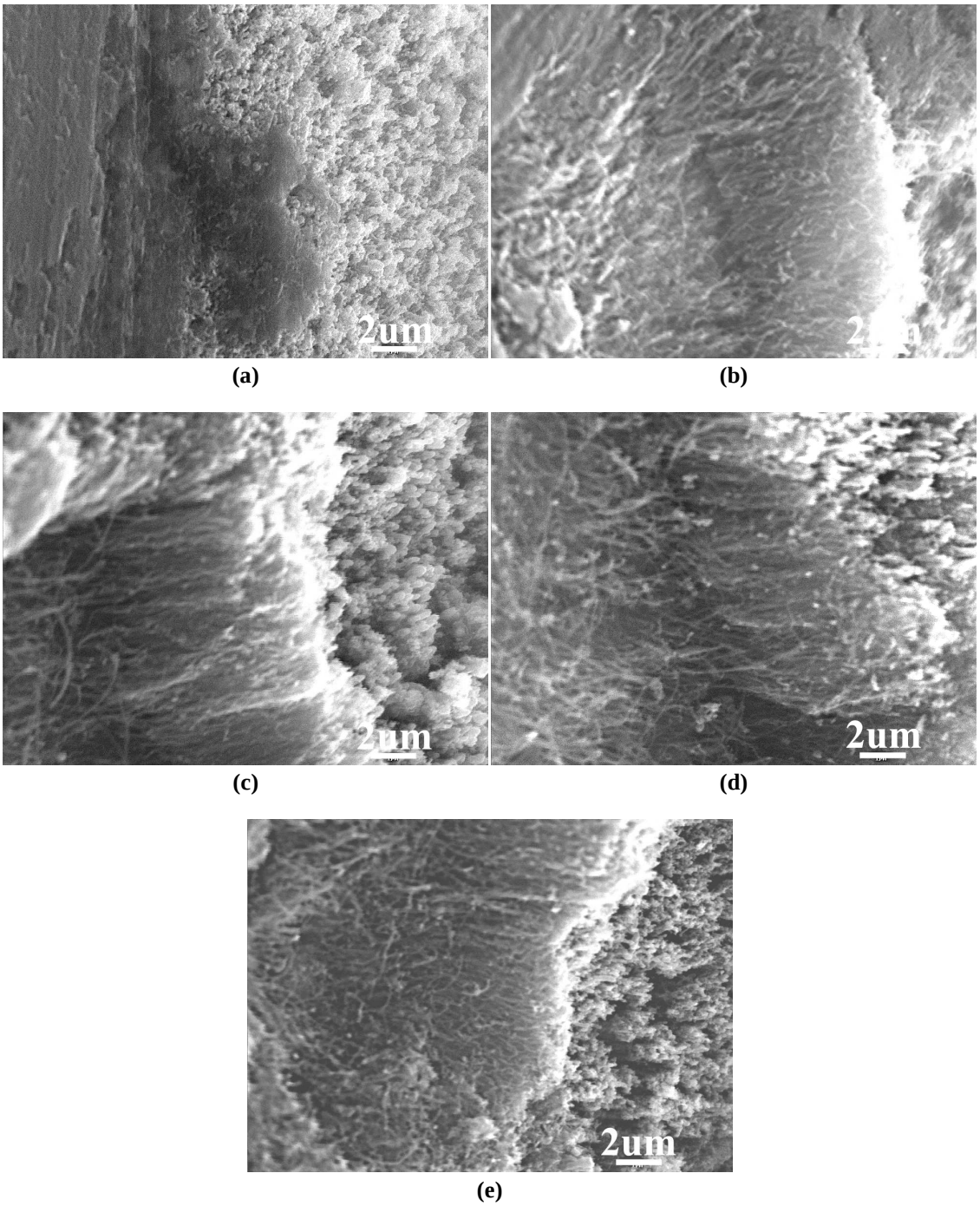

Figure 4.1: SEM surface morphologies of CNTs grown on as received Inconel plate (a), 800°C (b), 900°C (c), 1000°C (d), and 1100°C (e) pre-treated Inconel substrates. The scale bar is 2 μm

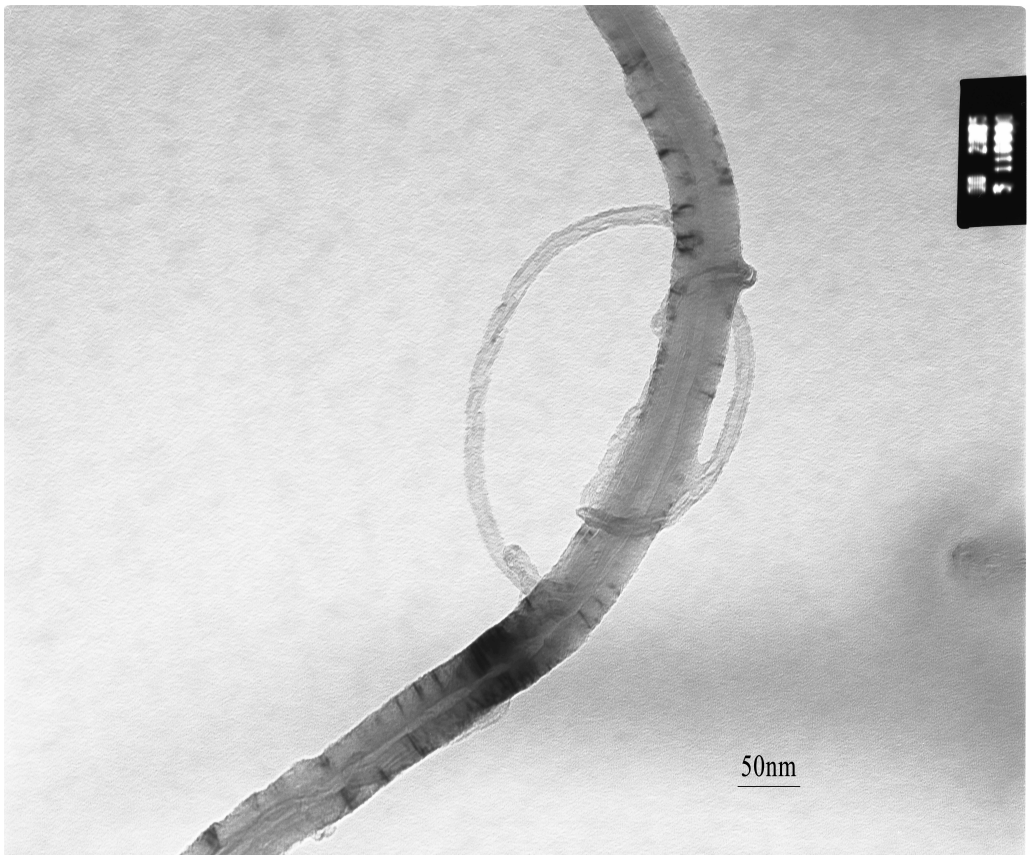

Figure 4.2: TEM image of CNTs grown on 1100°C pre-treated Inconel substrate.

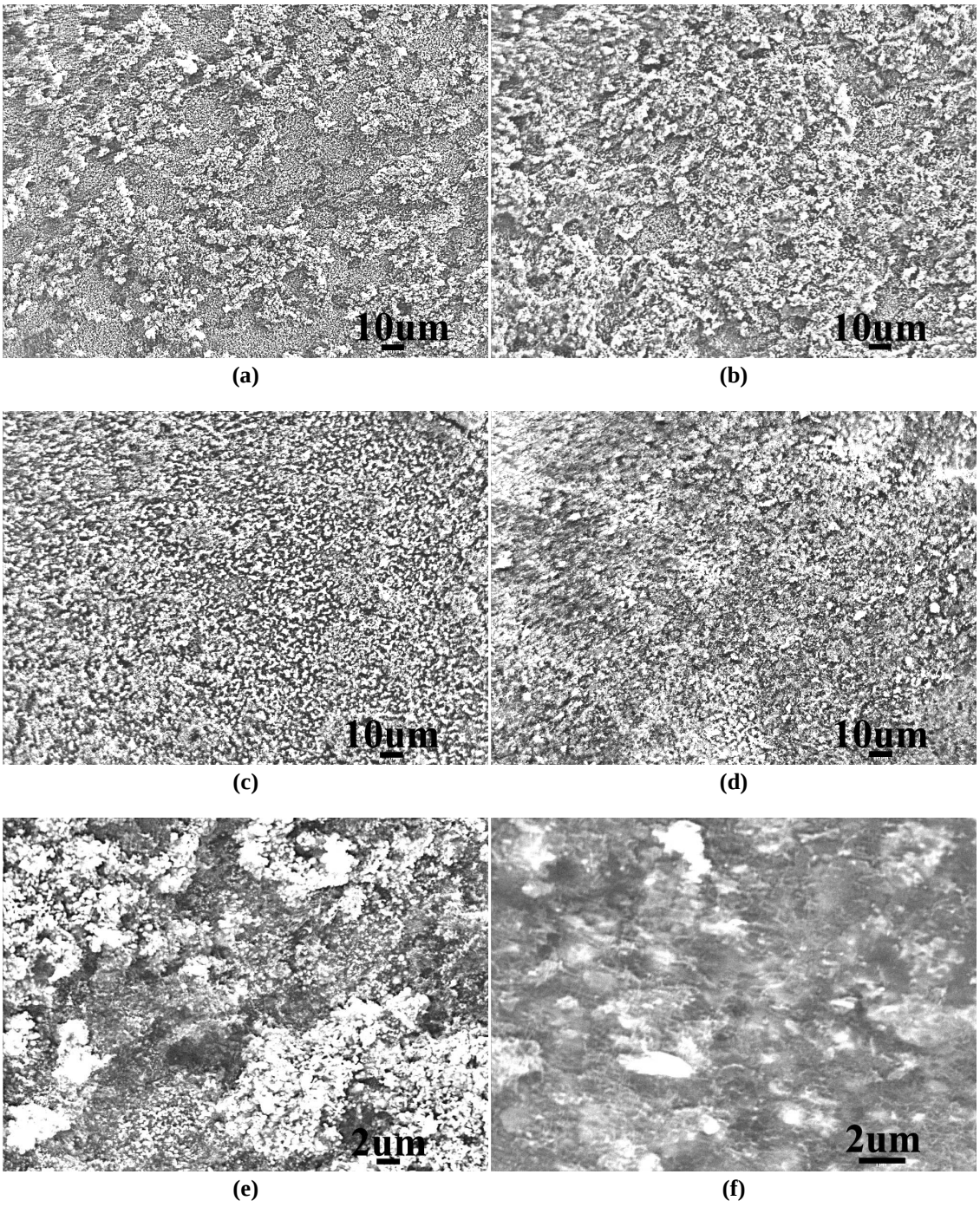

Figure 4.3: Top view SEM morphologies of samples deposited on different temperature pre-treated Inconel plates (800°C (a), 900°C (b), 1000°C (c), and 1100°C (d)); (e), (f) are pictures of sample (a) and (d) at higher magnification.

treated substrates, respectively. In Fig. 4.3f, carbon nanotube tips protrude from the crest face with only few noticeable particles located in between. In contrast, the top coverage in Fig. 4.3e consists of densely packed particles in a broad range of sizes.

In order to understand the effect of oxidation pre-treatment on the CNT growth, XRD and SEM have been applied to analyze the treated substrates before and after CNT deposition. Figure 4.4 shows the XRD patterns of the Inconel sheets before and after oxidation treatment at different temperatures. The results show that only a small amounts of Cr_2O_3 is present after oxidation at 800°C and 900°C, whereas various oxides including Cr_2O_3,Fe_2O_3, NiO, $NiCr_2O_4$ [136] appear after oxidation at 1000 and 1100°C and the amounts of oxides increase with the increase of pre-treatment temperature. Figure 4.5 presents the SEM images of the substrate after oxidation at different temperatures. The SEM images show that the substrate surface was roughened by oxidation pre-treatment regardless of the treatment temperature. As the oxidation temperature rose up, the grain boundaries became much clearer and the grains were extruded more out of the surface. Compared our XRD and SEM results with the reported literatures [136–138], we propose the oxidation procedures of the Inconel substrate as follows. Chromium (Cr) was the first element to be oxidized to form Cr_2O_3 because it needs lower partial pressure of oxygen to form oxide compared to the other two main elements: Ni and Fe in the alloy [137]. Cr_2O_3 nucleates and grows preferentially along the alloy grain boundaries due to their high energy and high diffusion rate, thus Cr_2O_3 islands formed along alloy grain boundaries [136, 138]. At higher oxidization temperature, Cr_2O_3 islands continued to grow while other oxides like NiO started to nucleate and grow at the alloy surface. Eventually, a continuous Cr_2O_3 layer may form at the bottom of other oxides [136, 138], uplifting the other oxides out of the surface.

Once methane and hydrogen were introduced for CNT deposition, different reactions happened on differently pre-treated substrates. XRD patterns of the samples after CNT deposition are shown in Figure 4.6. Comparing Figure 4.6 with Figure 4.4, we can see that graphitic carbon (CNTs) has been grown on all the samples after deposition as the representative peak of graphitic (002) at around 26° is observed after deposition [139–142]. Cr_2O_3 was not reduced during the deposition process as Cr_2O_3 shows similar peak in-

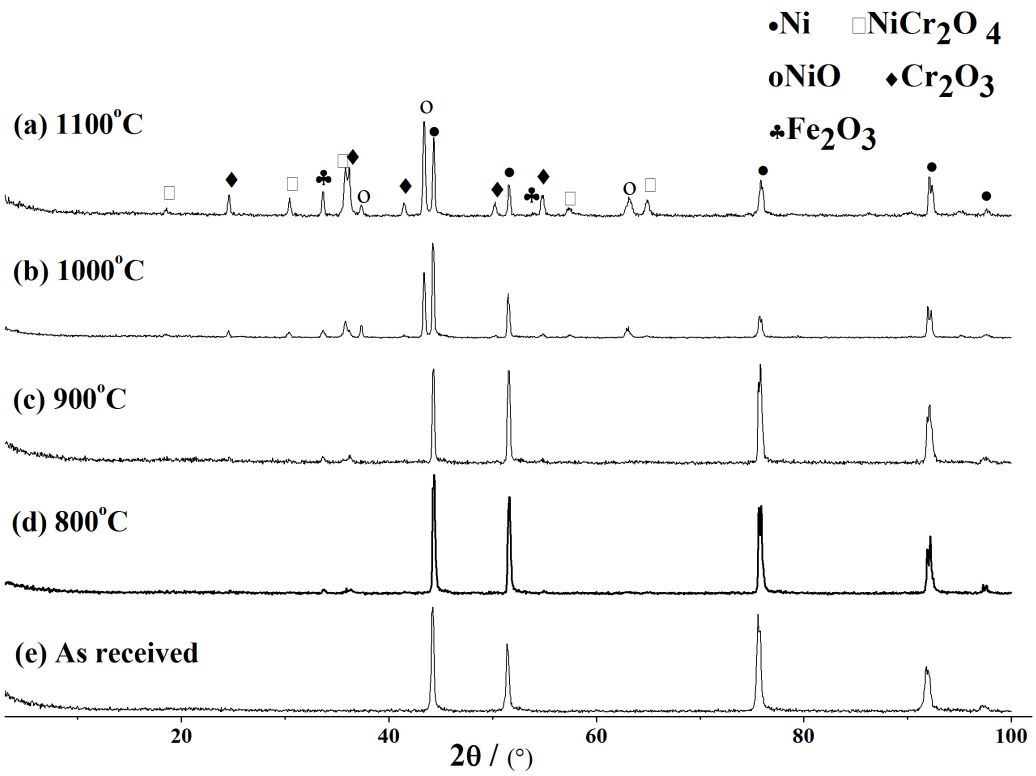

Figure 4.4: XRD patterns of as received and oxidized Inconel plates.

tensity in XRD patterns before and after deposition. Some oxides, including NiO and $NiCr_2O_4$, formed at higher oxidation temperature might be reduced to metallic state after the deposition as the diffraction peaks for these oxides disappears after CNT deposition. Since there is no reduction of Cr_2O_3, the oxidation-reduction catalyst generation mechanism is not applicable for 800 and 900°C pre-treated samples. We can ascribe the CNT growth on 800 and 900°C pre-treated substrates to thermal stress roughing, in which the roughed surface provides catalytically active sites for CNT growth [6]. The thermal effect should also play roles for CNT growth on the samples pre-treated at 1000 and 1100°C. However, for samples pre-treated at 1000 and 1100°C, the other mechanisms including oxidation-reduction catalyst generation should also be considered. At higher oxidation temperature, more oxides were produced, which may induce the formation of more edge sites and hamper the formation of bigger catalyst clusters [143]. Meanwhile, some oxides, including NiO and $NiCr_2O_4$, formed at higher oxidation temperature were reduced to metallic state to form active catalyst particles for CNT growth during the deposition.

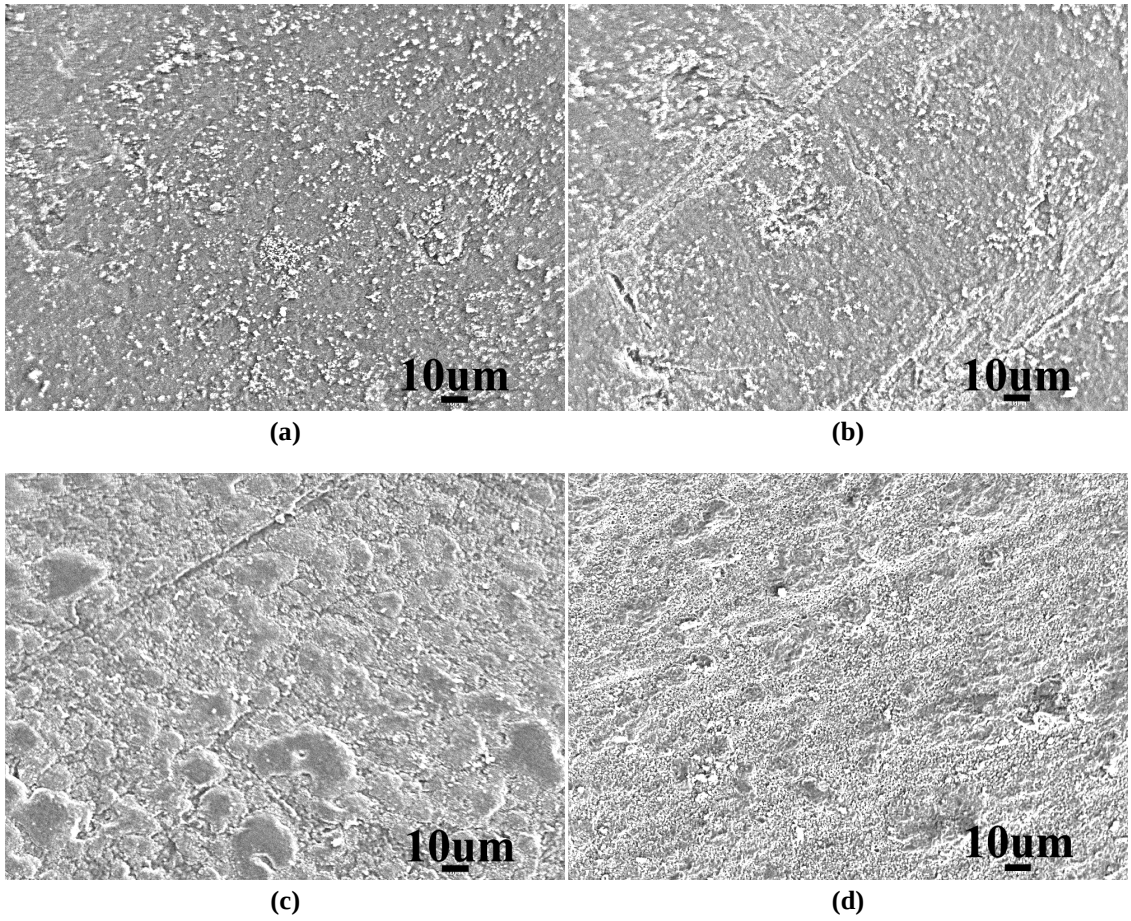

Figure 4.5: Surface morphologies of Inconel substrates after oxidation under different temperatures (800°C (a), 900°C (b), 1000°C (c), and 1100°C (d)).

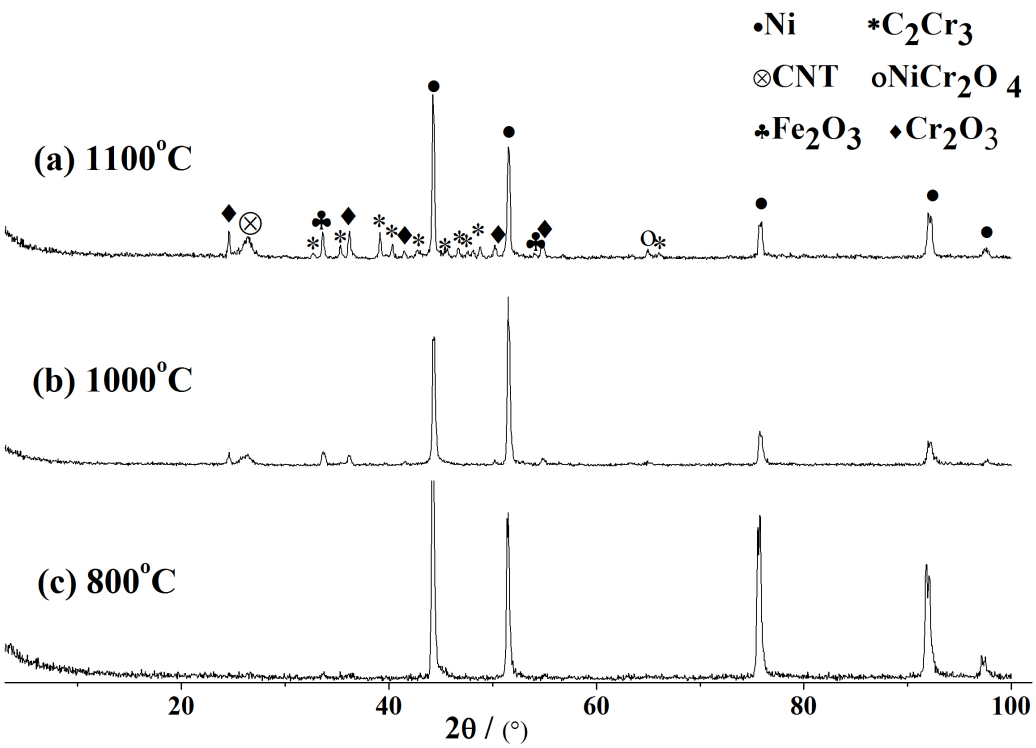

Figure 4.6: XRD patterns of oxidized Inconel plates after deposition.

In addition, a continuous Cr_2O_3 layer might form at the bottom of the other oxides at higher oxidation temperature and act as a supporting layer for the creation of catalyst particles through reduction [142, 144]. On this supporting layer, the catalyst particles formed would be better separated and more uniformly distributed, resulting in CNTs with better uniformity [121]. Based on above analyses, the higher oxidation temperature would facilitate CNT growth with better uniformity, which is in agreement with the SEM results shown in Fig. 4.1 and 4.3 and further confirmed by XRD patterns shown in Figure 4.6 and Raman spectra presented in Figure 4.7. From Figure 4.6, we can see that the higher the oxidation temperature, the higher and the sharper the graphite peak ($\sim 26^\circ$) resulted from CNTs. From Figure 4.7, we can see that the I_G/I_D ratio in Raman spectra increases with the increase of oxidation temperature, where higher I_G/I_D ratio indicates CNTs with more perfect structure [111].

It is also worthy to note that few Fe_2O_3 are reduced by comparing Fig. 4.6 with Fig. 4.4. We can assume that it works together with Cr_2O_3 as catalyst support. At lower

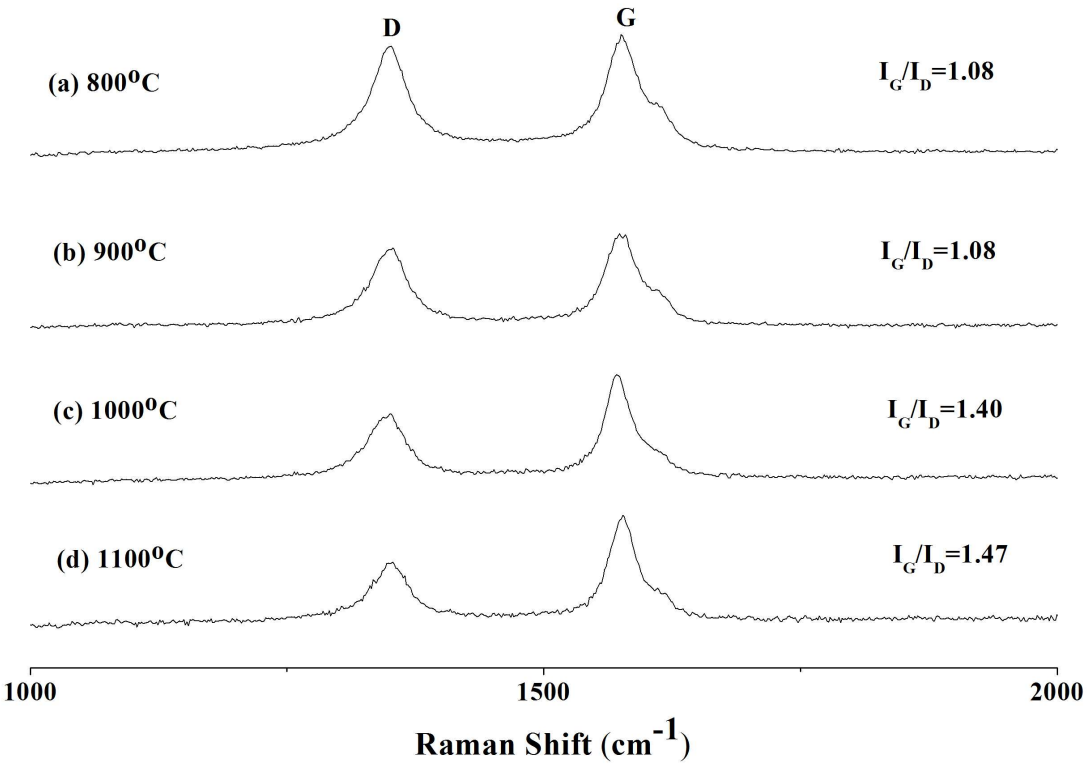

Figure 4.7: Raman spectra of CNTs grown on Inconel substrates pre-treated under different temperatures.

temperature (800 and 900°C), fewer Fe_2O_3 was formed, indicating more Fe might join with Ni in catalyzing CNT growth, thus with the increase of oxidation temperature, the active CNT catalysts would contain higher concentration of Ni. It has been reported that Ni promotes the growth of straight CNTs whereas Fe facilitates the growth of twisted or crooked CNTs [121, 145]. Then the CNTs grown on substrates with higher oxidation temperature would be more straight and well aligned, which is evident in SEM images shown in Fig. 4.1. Furthermore, a new phase C_2Cr_3 was formed for 1100°C pre-oxidized sample, as seen from XRD patterns in Fig. 4.6. The new compound is anticipated to further improve the interaction between substrate and the newly formed catalyst and to lead to fewer particles on the top of CNTs, as seen in Fig. 4.1e and Fig. 4.3f.

Fig. 4.8a presents the field electron emission I-E curves of the deposited CNT samples. For the CNT film grown on 800°C pre-oxidized Inconel substrate, the largest turn-on electric field (defined as the electric field at which the emission current reaches 0.01 μA) of 6.56 V/μm is obtained. With the increase of the oxidation temperature from 800°C, the deposited CNTs exhibit decreased turn-on electric field of 5.78 V/μm at 1000°C and 4.66 V/μm at 1100°C. The Fowler-Nordheim (F-N) plot corresponding to the field emission I-E curve for each sample is displayed in Fig. 4.8b. Using the work function of 5 eV for CNTs [146], the field enhancement factor β was estimated from the slope of the FN plot. The largest β is achieved from the sample with 1100°C pre-treatment. It decreases from 872 to 693 and 626 when the oxidation temperature decreases to 1000°C and 800°C. Sung *et al.* [147] have observed the similar effect of CNTs uniformity on their FEE properties. They used a glass cap to level the CNTs height and found that the vertically levelled CNTs showed better field emission characteristics than unlevelled ones.

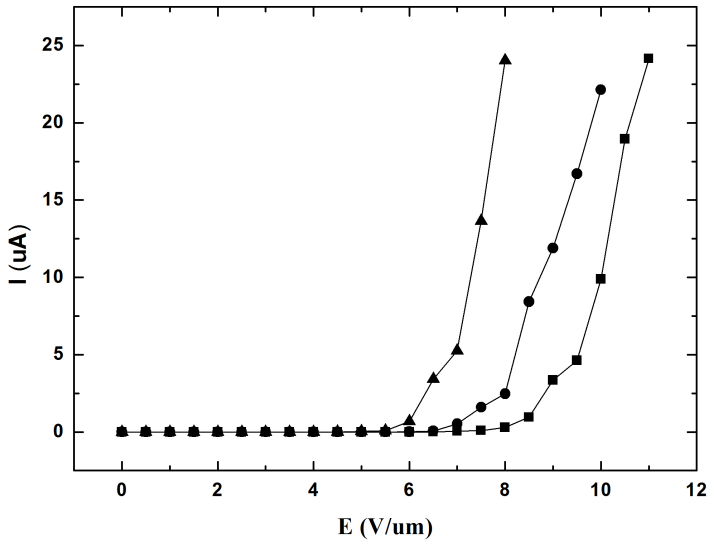

(a) Typical FEE I-E curves.

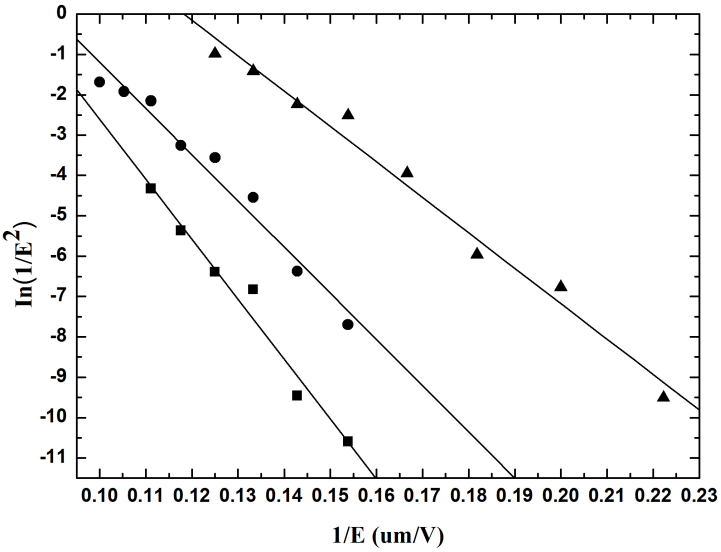

(b) Typical FEE FN curves.

Figure 4.8: FEE tests of CNTs grown on pre-treated Inconel plates (■ pre-treat temperature 800°C; ● pre-treat temperature 1000°C; ▲ pre-treat temperature 1100°C).

4.2 The secondary growth of carbon nanotubes by simply adjusting carbon concentration during deposition and its effect on FEE properties

Figure 4.9 shows surface morphologies of 1100°C pre-oxidized Inconel substrates after CVD process in an extremely low carbon concentration (0.28 vol.%) gas environment for 10 min, 30 min, and 1 hour. After 10 min processing, the substrate surface is characterized by irregular large particles with small protuberances distributed on the top of them (Fig. 4.9a). 30 min processing results in the reduced particle size with very fine particles centered at the particle boundaries (Fig. 4.9b). After 1 h CVD process, however, filamentous structure is observed (Fig. 4.9c). TEM observations of the samples after 1 h processing confirm that filamentous structure consists of CNTs. Fig. 4.10 shows a TEM image of a typical CNT. It is a centrally hollow tube, rather than a fiber. As can be seen from the figure, the outer diameter of this CNT is approximately 35 nm. The inner diameter is approximately 5 nm, and many catalyst nano particles are embedded in the walls and/or within the hollow space of the tubes. These catalyst nano particles, just like those intentionally deposited catalyst nano particles on primary CNTs, are supposed to catalyze the secondary CNT growth during the consequent CVD process at higher methane concentration. The metal dusting theory can be used to explain the observed results. As reported, there are two metal dusting mechanisms working conjointly for Ni-based alloys [148]: one is that carbon diffuses into metal and eventually leads to carbon precipitation, which disintegrates the carbon supersaturated metal particle, thus resulting in a reduction of catalyst particle size; the other one involves selective oxidation of carbides formed during the processing, in which metal dust and metal oxides forms. The dusted metal particles are blown onto the growing carbon nanotubes and attached to the CNT walls, especially those defect sites caused by hydrogen etching, resembling catalyst seeding for secondary CNTs. Figure 4.11 shows the XRD patterns of the oxidized Inconel sheets before and after deposition at carbon concentration of 0.28 vol.% for different time durations. After 10 minutes deposition (CVD processing), the oxides NiO and $NiCr_2O_4$ formed during the

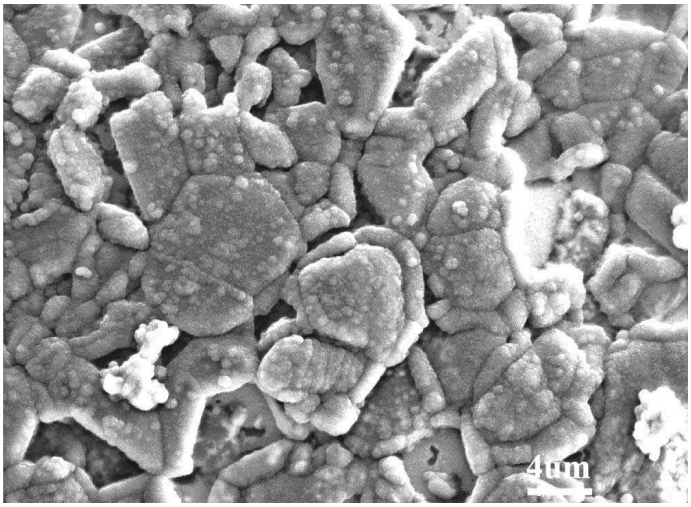

(a)

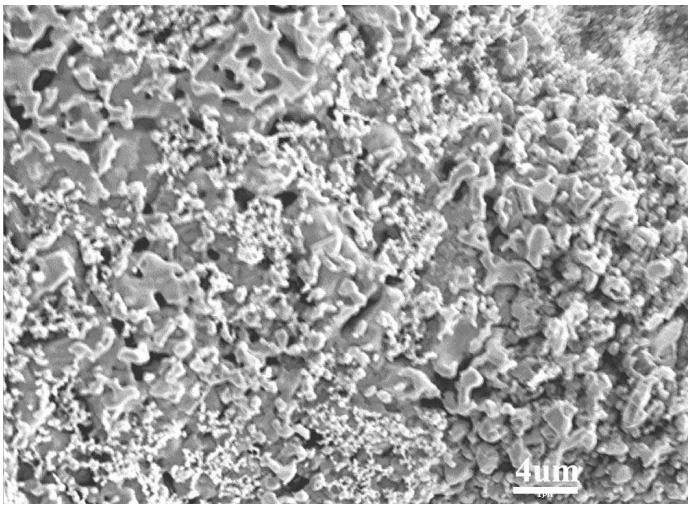

(b)

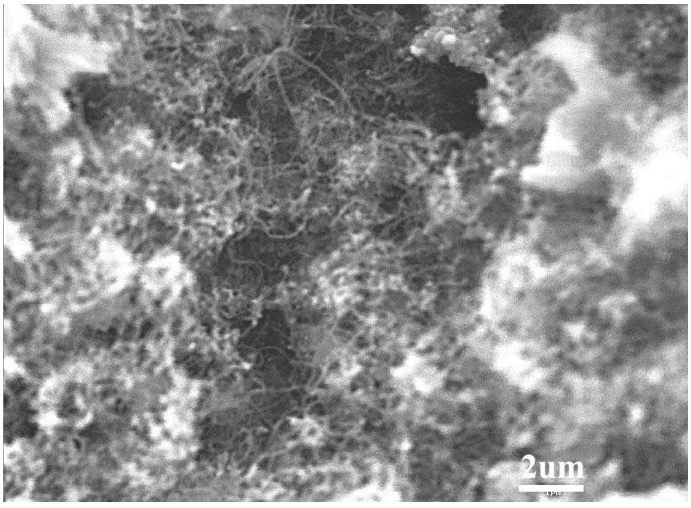

(c)

Figure 4.9: surface morphologies of pre-oxidized Inconel substrates after CVD process in extremely low carbon concentration gas environment for 10 min (a), 30 min (b), and 1 hour (c).

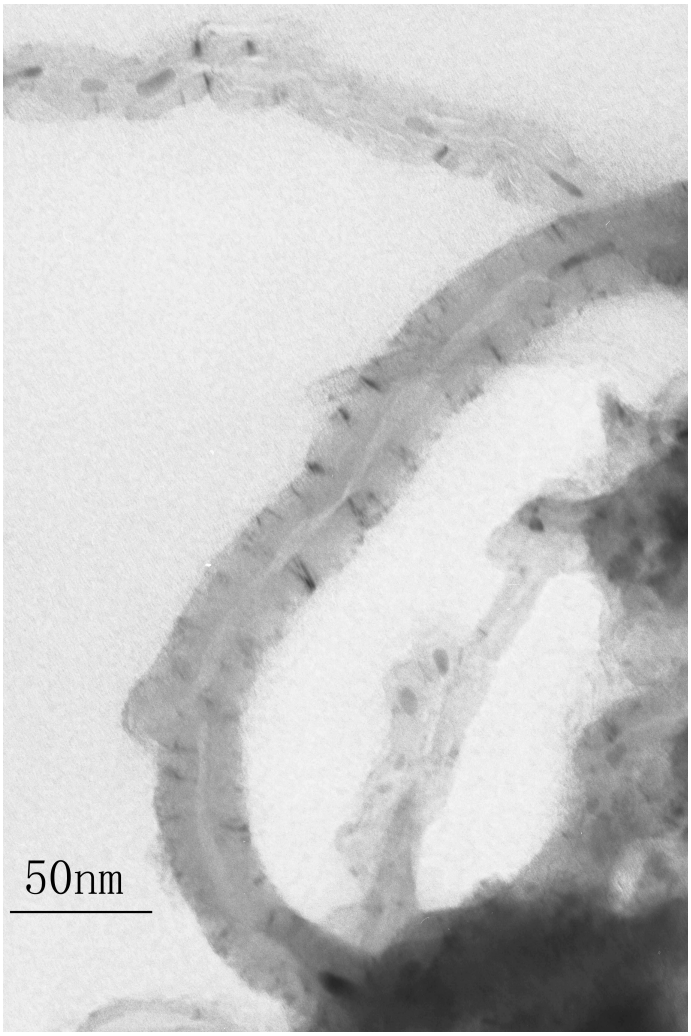

Figure 4.10: TEM characterization for the CNT sample grown at carbon concentration of 0.28 vol.% for 1 h.

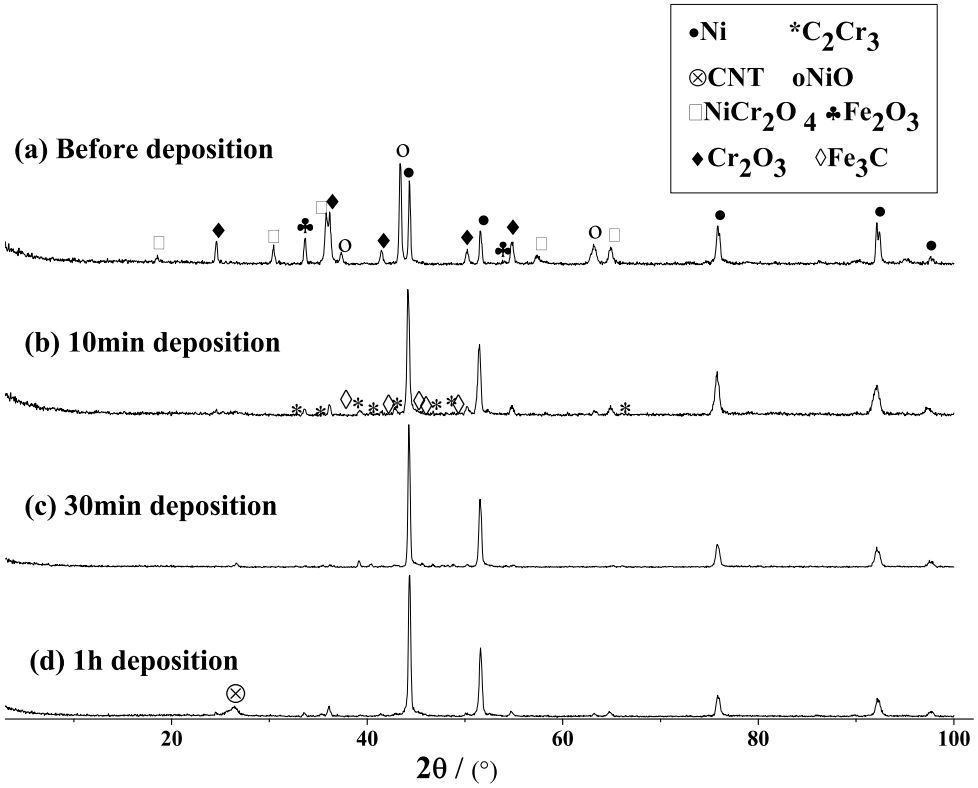

Figure 4.11: XRD patterns of oxidized Inconel plates before deposition and after deposition at carbon concentration of 0.28 vol.% for different time durations.

pre-treatment were reduced and carbon has begun to dissolve into metal particles, forming iron and chromium carbides. Since carbon diffuses fast in nickel and that nickel carbide is not a necessary intermediate product [149], we assume that the disintegration mechanism is dominant in the early stage. When the CVD duration was extended to 30 minutes, oxygen or hydrogen starts to play roles. It reacts with the carbides formed during the early stage of CVD processing to form metal dust, evident from the diminished carbides peaks, as shown in Fig. 4.11(c), whereas disintegration mechanism, super saturation-precipitation-disintegration course, occurs simultaneously. The oxygen may be originated from the reduction of pre-formed oxides and the residual air, whereas hydrogen was flowing into the system during the deposition. As the CVD process proceeded to 1h, a strong peak at around 26° emerged, indicating the CNT growth [139, 141]. This is consistent with the SEM observation in Fig. 4.9. Meanwhile, the metal dusting was continuously carrying on, evident from the disappeared diffraction peaks of carbides, as shown in Fig.4.11(d). To investigate the uniqueness of CVD synthesis at extremely low carbon concentration, the growth of primary carbon nanotubes has also been conducted under higher carbon concentration conditions (5 vol.%). It has been found that the growth of CNTs becomes much faster. Carbon nanotubes had already formed within 10 minutes processing, as shown in Fig. 4.12 and Fig. 4.13. But catalyst nano particles were barely observed on CNT walls for 1 h processed samples. TEM image of a typical CNT from the 1h processed samples is shown in Fig. 4.13. The outer diameter of the CNT (approximately 50 nm) is larger than that grown at 0.28 vol.% carbon concentration. In this case, the small metal particles were exhausted quickly for CNT growth and the synthesized CNTs covered the surface to prevent the metal dust formation. In addition, less defect sites are created on the walls due to the decreased hydrogen content. As anticipated, the extended CVD process did not produce any secondary CNTs.

For the secondary CNT growth, higher carbon concentration (5 vol.%) was applied to the primary CNTs obtained using extremely low carbon concentration (0.28 vol.%) CVD processes. Figure 4.14a shows the SEM micrograph of the secondary growth products. Small CNT sprouts are protruding out of the surface. The TEM observations (see Fig. 4.14b) shows that smaller and shorter secondary CNTs wind along thicker and longer

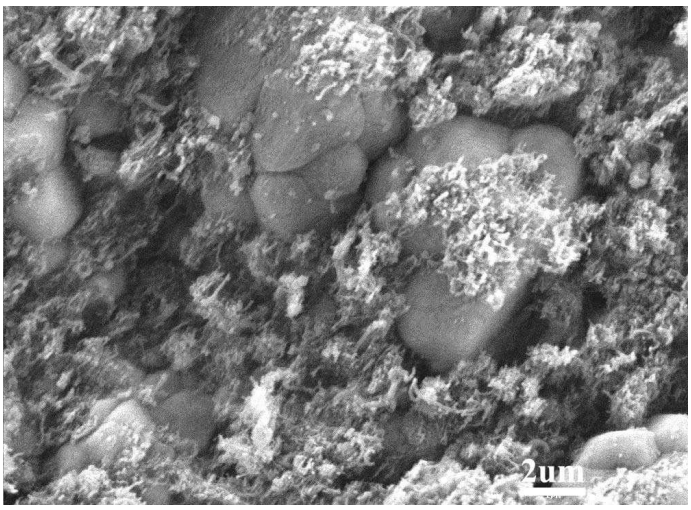

Figure 4.12: Deposits on Inconel substrate at carbon concentration of 5% after 10min growth.

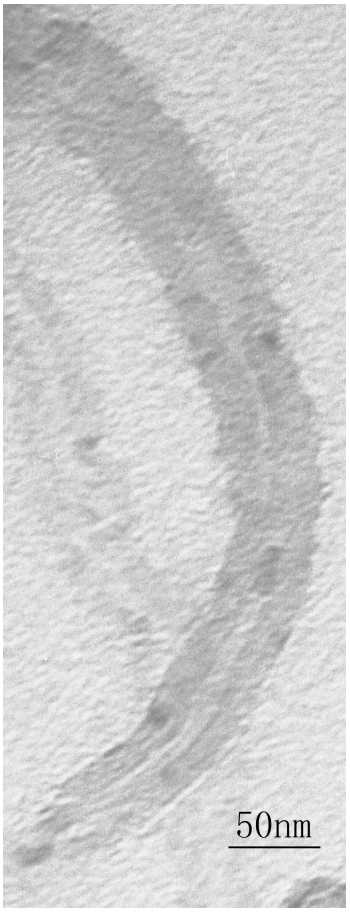

Figure 4.13: TEM characterization for the CNT sample grown at carbon concentration of 5 vol.% for 1 h.

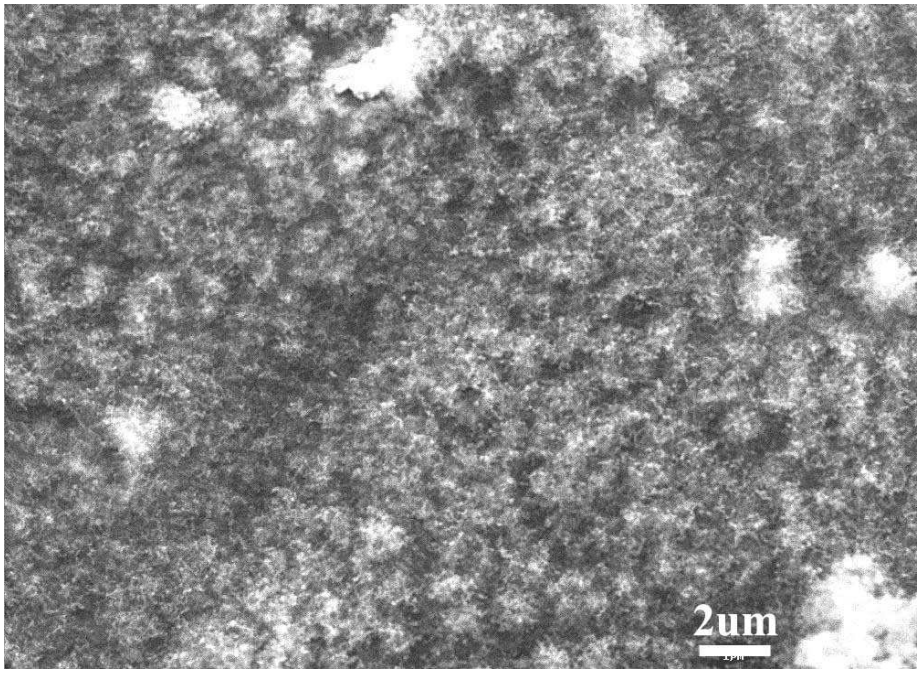

(a)

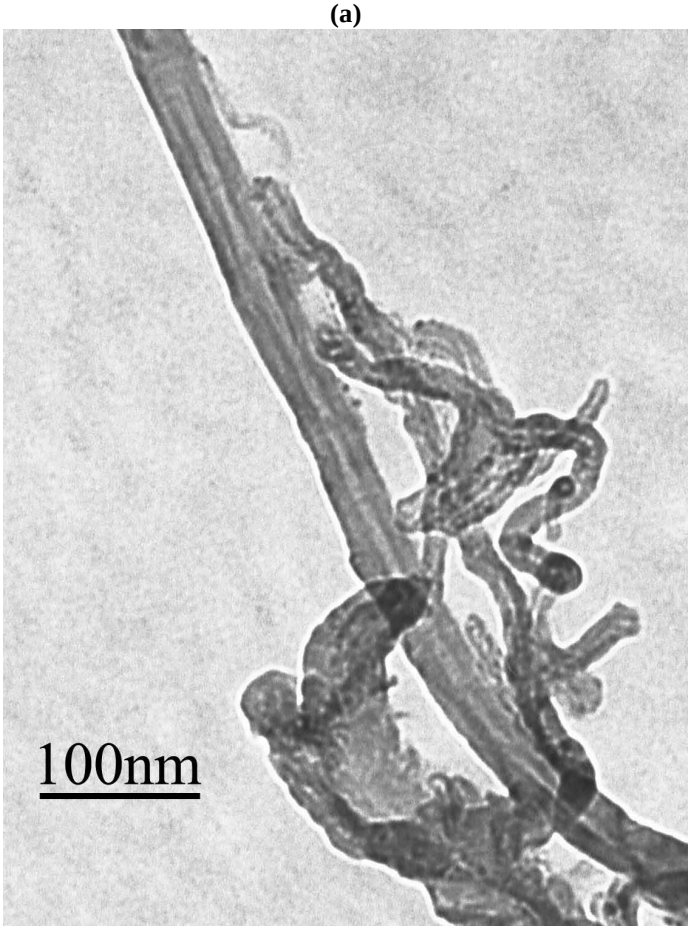

(b)

Figure 4.14: SEM (a) and TEM (b) characterization of the secondary growth product.

primary CNTs. The outer diameter of the secondary CNTs was estimated to be in the range of 8 to 15 nm. Field electron emission properties were also tested for both the primary CNTs and the binary structure combing thick primary CNTs and thinner secondary CNTs, as well as the CNTs grown under regular carbon concentration.

Fig. 4.15a presents the field electron emission I-E curves of the samples. The Fowler-Nordheim (F-N) plot corresponding to the field emission I-E curve for each sample is displayed in Fig. 4.15b. Assuming the work function of 5 eV for CNTs [146], the field enhancement factor β is estimated from the slope of the FN plot. The primary CNTs synthesized from extremely low carbon concentration have a turn-on electric field (defined as the electric field at which the emission current reaches 0.01 μA) $\mathrm{E_{to}}$ = 3.50 V /μm, with the field enhancement factor $\beta = 1213$. The growth of secondary CNTs leads to improved field emission properties ($\mathrm{E_{to}}$ = 2.28 V/μm, and a larger emitted current density for a certain applied electric field). The improvement may be associated with the smaller diameter of the secondary CNTs which would emit electrons at a low voltage [150, 151]. Different from other reports on the degraded field amplification factor caused by the short length of the secondary CNTs [152], in our case, no worsening effect was observed after the secondary growth ($\beta = 1577.8$). The negative influence resulted from the short length of the secondary nanotubes may have been eliminated by the smaller diameter of the secondary CNTs. The sample with the CNTs grown at regular carbon concentration (5 vol.%) without secondary nanotubes shows an inferior FEE performances comparing with the other two ($\mathrm{E_{to}}$ = 4.09 V/μm, $\beta = 979.4$). We ascribe this to the less defects on the side walls,thus less emission sites.

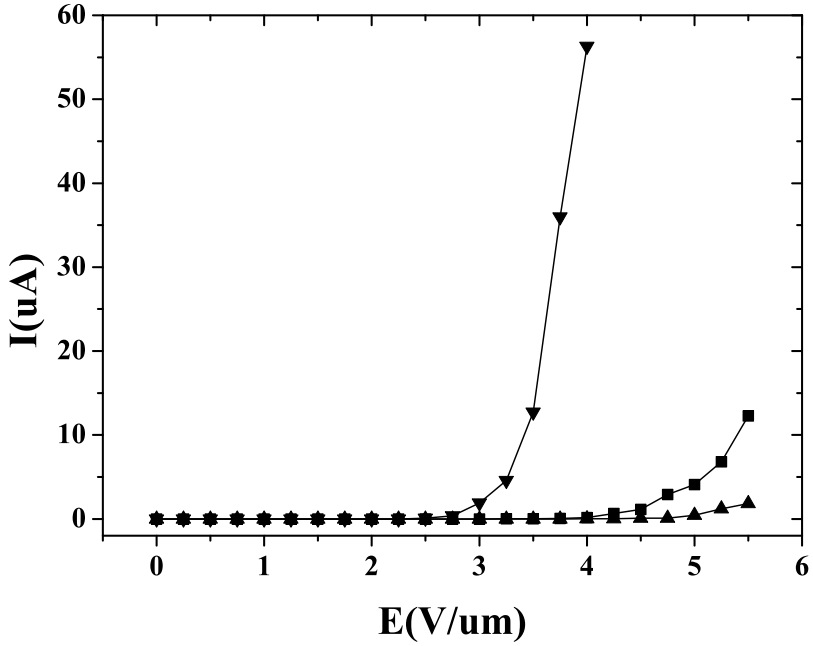

(a) Typical FEE I-E curves.

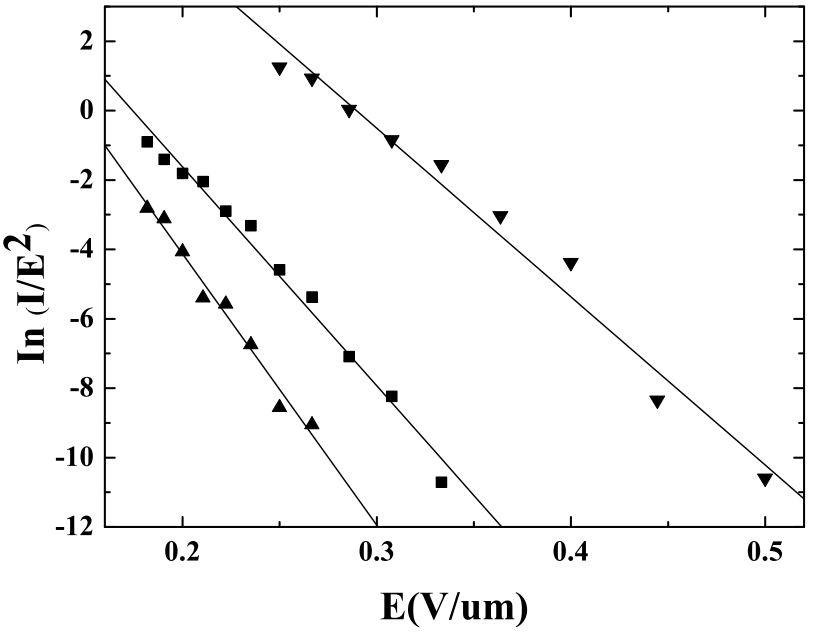

(b) Typical FEE FN curves.

Figure 4.15: FEE tests of CNTs grown under different conditions (■ primary CNTs under extremely low carbon concentration; ▼ combined structure of primary and secondary CNTs; ▲ CNTs grown under regular carbon concentration.

4.3 The effect of bias on aligned carbon nanotube growth and alignment mechanism of carbon nanotubes by hot filament chemical vapor deposition

The as-received Inconel sheets were pre-heated and then used as substrates for direct growth of carbon nanotubes under various bias voltages ranging from -550 V to +150 V. The SEM morphologies of the resulted deposits under different bias voltages are shown in Fig. 4.16. It can be seen that aligned CNTs were produced under both positive and negative substrate bias, whereas only random CNTs were obtained when the substrate bias = 0 V, indicating that biasing during the growth is critical in aligning nanotubes. Biasing of the substrate has been widely used in CNT growth. But the question of which bias (positive or negative) is more effective for nanotube alignment still remains unclear. Avigal *et al*. [119] found that positively biasing the substrate enhanced the alignment performance. Zhang *et al*. [22] demonstrated a similar performance with positive dc bias and ac bias. Negative self biasing of the substrate in a plasma was also effective for nanotube alignment as reported by Bower *et al*. [21, 26]. In this paper, both positive and negative biases have been investigated. From Figure 4.16, one can find that the CNTs grown at -500V shows the best alignment. Among the negatively biased growths, the one with -500V bias shows the best result. Below -500V, CNTs are less straight. Beyond -500V, CNTs are so densely packed that their heads are fused together and formed into a cap shell, caused by higher temperature from higher plasma intensity. Thus -500V bias was adopted for other experiments in this section.

Figure 4.17 shows the SEM images of the samples prepared with a growth time of 10 min and 30 min under a bias of -500 V. The SEM image of the 1h grown sample can be found in 4.16e. It is interesting that the randomly distributed and aligned CNTs present simultaneously after 10 min growth (Fig. 4.17a). This is not consistent with the reported results which support the electric field induced alignment mechanism [29, 30]. Therefore, electric field may not be the only factor determining the CNT orientation. Merkulov *et al*. [23–25] have reported the formation of both aligned and nonaligned CNTs

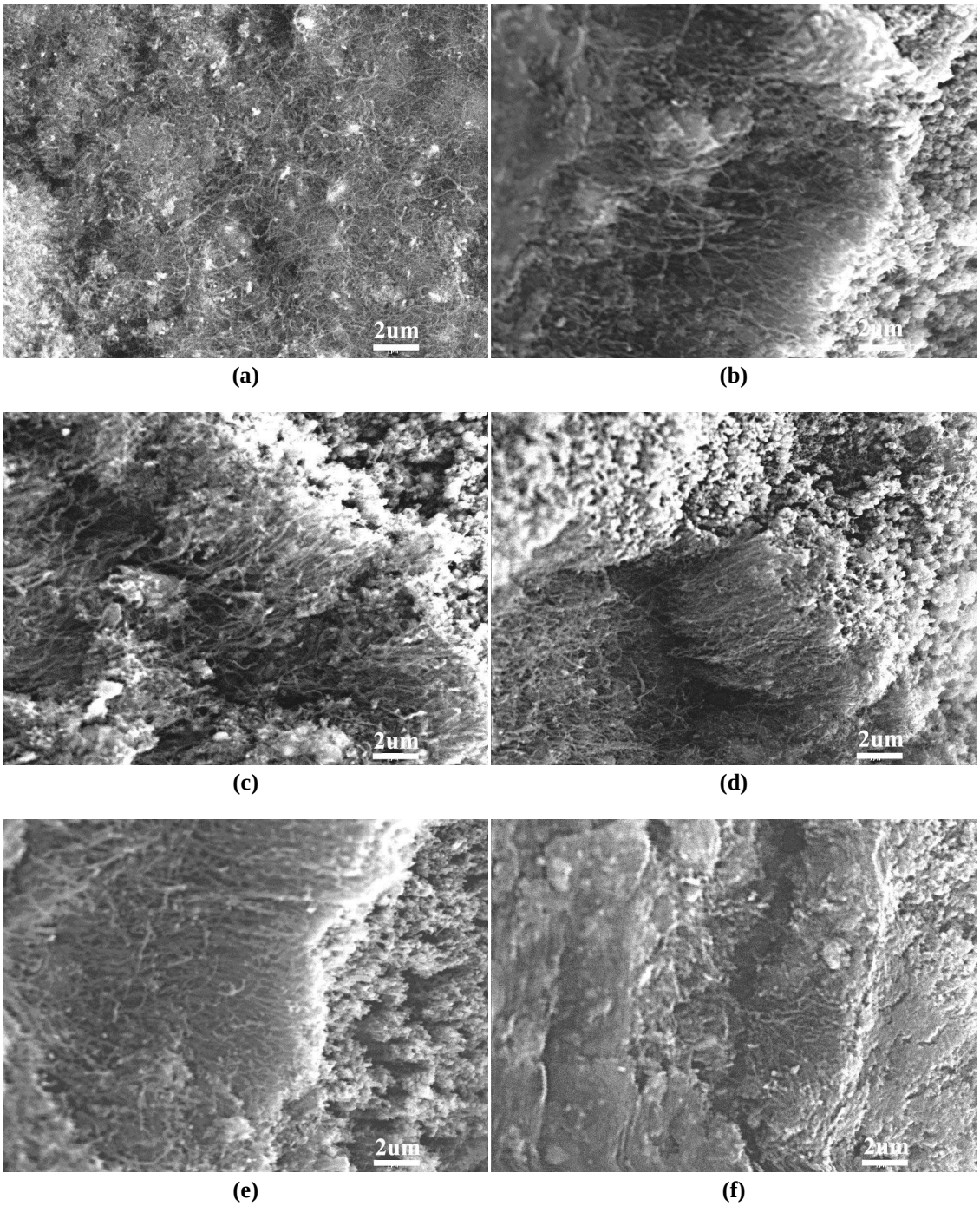

Figure 4.16: SEM morphologies of deposits on pre-oxidized unscratched Inconel plates under different bias (0V (a), 150V (b), -400V (c), -450V (d), -500V (e), and -550V (f)). The scale bar is 2 μm.

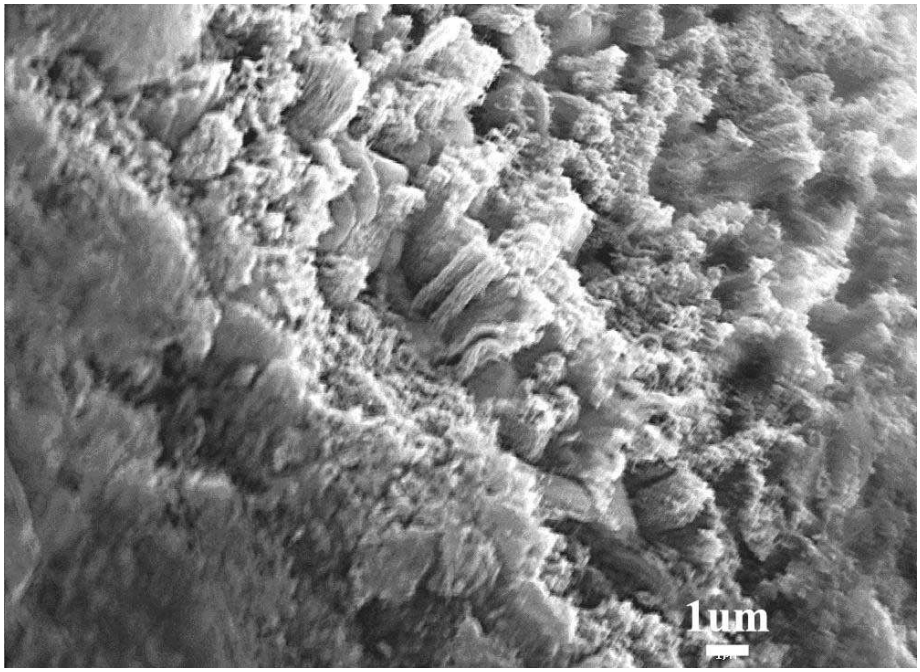

(a)

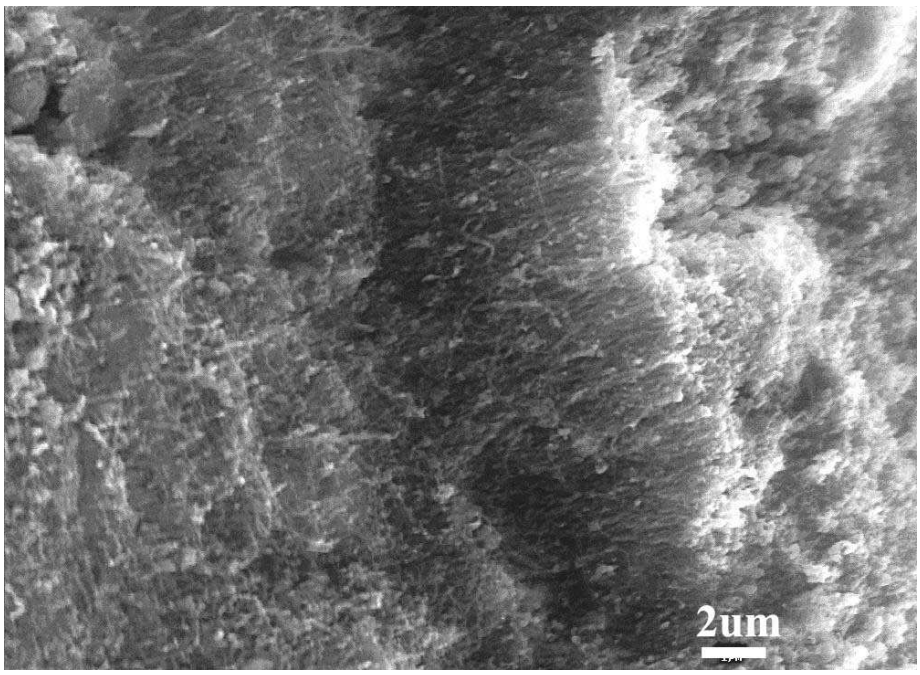

(b)

Figure 4.17: SEM morphologies of samples prepared under -500V with different growth time (10 min (a), 30 min (b)).

in one single growth process. The mechanism was given as follows: different stresses are produced by electrostatic force between tip growth and base growth, consequently leading to differences in carbon diffusion and precipitation; the growth with catalytic particle at tube tip is favorable for alignment whilst the base growth causes misalignment. In our case, TEM observation of the samples with 10 min growth (Fig. 4.18) reveals mixture of tip growth and base growth (with an open end). Therefore, the stress related mechanism, supposed by Merkulov *et al*. [23–25] can well explain the observed co-growth of randomly distributed and aligned CNTs here. As seen in Fig. 4.17b and Fig. 4.16e, only aligned CNT arrays were observed for samples after 30 min or 1h growth, indicating that crowd effect eventually makes the randomly distributed CNTs into aligned arrays.

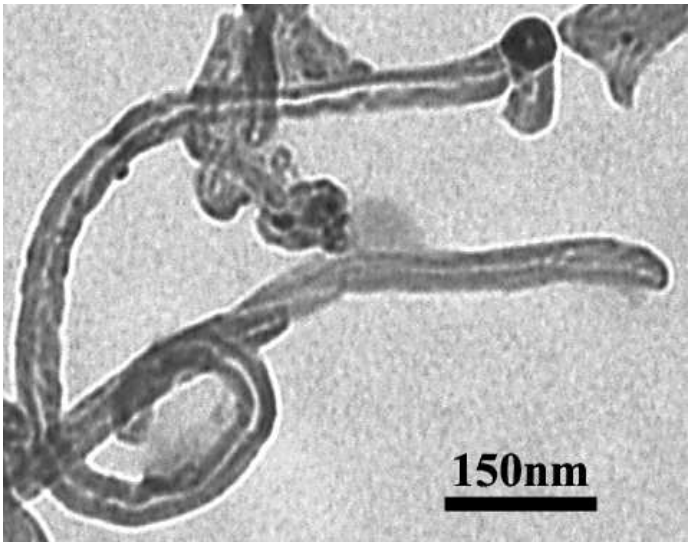

Figure 4.18: TEM characterization of 10 min grown sample under bias of -500 V.

Besides electric field, many researchers have found that other deposition conditions such as gas composition, catalyst type, catalyst layer thickness can also affect the alignment in CNT growth [33]. In this section, Inconel sheets mechanically scratched before the heat treatment were also used for CNT growth. Figure 4.19 presents the SEM morphology of the resulted CNTs. Unlike CNT forest shown in Figure 4.17, isolated tree-like CNT structure is displayed. The CNTs grown in the center, right upper corner, and right bottom corner of the substrate were shown in Fig. 4.19a, 4.19b, and 4.19c, respectively. It is interesting that the deviation of the tube axis from the substrate normal near the sample edges. This phenomenon has previously been reported by Yang *et al*. [105] and Merkulov *et al*. [25] The axis derivation has been ascribed to the derivation of electric field line. The CNTs grown on the unscratched substrates shown in Fig. 4.16 exhibited similar alignment characteristic, although it is harder to observe due to the high packing density. Figure 4.20 shows the SEM morphology of CNT on scratched substrates after 10 min growth. It shows that tens of freely standing nanotubes are outgrown unevenly from one catalyst dot. TEM observation of the CNTs scratched from the substrate shows similar features as in Fig. 4.18. Comparing Figure 4.19 to 4.20, it is suggested that the carbon nanotubes are initially aligned by electrostatic force, then as the growth proceeds, the van der Waals force interacts within a bundle of CNTs and makes them into a tree-like structure. It is

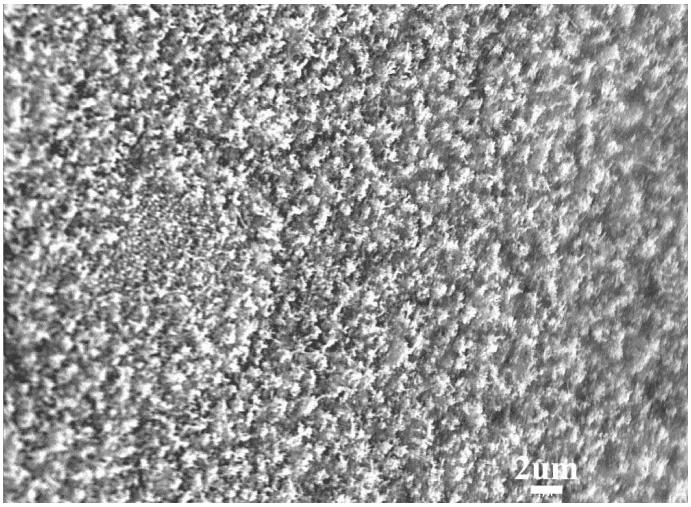

(a)

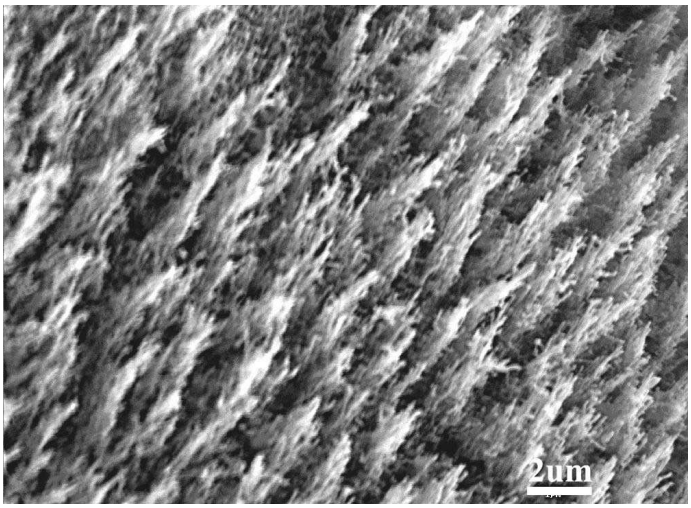

(b)

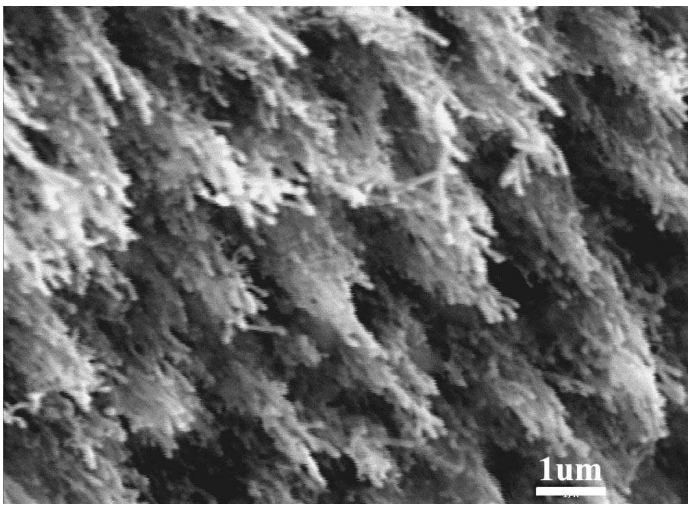

(c)

Figure 4.19: SEM morphologies of deposits on scratched substrates at -500V and growth time of 1h. The pictures were taken at different spots on substrate (center (a), right upper corner (b), and right bottom corner (c)).

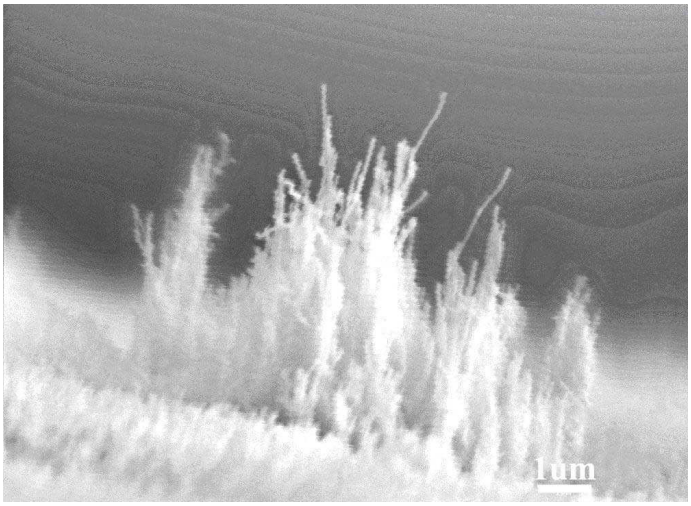

Figure 4.20: Early stage of carbon nanotubes grown on scratched substrate. The scale bar is 1 μm.

worthy to note that the tube diameter in Fig. 4.19 (90 $\sim$ 100 nm) is apparently larger than that in Fig. 4.17 (diameter: 50 $\sim$ 60 nm). It should be noted that at the initial growth stage, no randomly distributed CNTs were grown on the scratched substrates even though both tip and base growth were observed for the scratched substrates, indicating that having catalyst particle in tip is not indispensable for aligned growth in electric field. In addition, the heights of the aligned tubes on the scratched substrates are uneven (Fig. 4.19), different from the case in Fig. 4.17a. To explain these discrepancies, heat treated substrate surface morphologies with and without pre-scratching observed by SEM were compared, as shown in Fig. 4.21. After scratching, fairly deep tracks are left on the surface. The particles formed on the scratched substrate after heat treatment exhibit larger average size ($\sim$ 1 μm) and thinner distribution than unscratched ones (average grain size: $\sim$ 0.6 μm). Previous researches have found that big catalyst particles promote the alignment of CNTs and large catalyst size distribution causes fluctuation in heights of the formed tubes [121]. Thus we can attribute the above discrepancies between the scratched and unscratched substrates to the bigger particle size and larger particle size distribution on the scratched Inocnel sheets and the results show that as long as the catalyst size is big enough, it is possible to grow well-aligned carbon nanotubes in base growth mode.

The field emission properties were measured and the results are given in Table 4.1. The turn-on field of each sample is defined as the electric field at which the emission

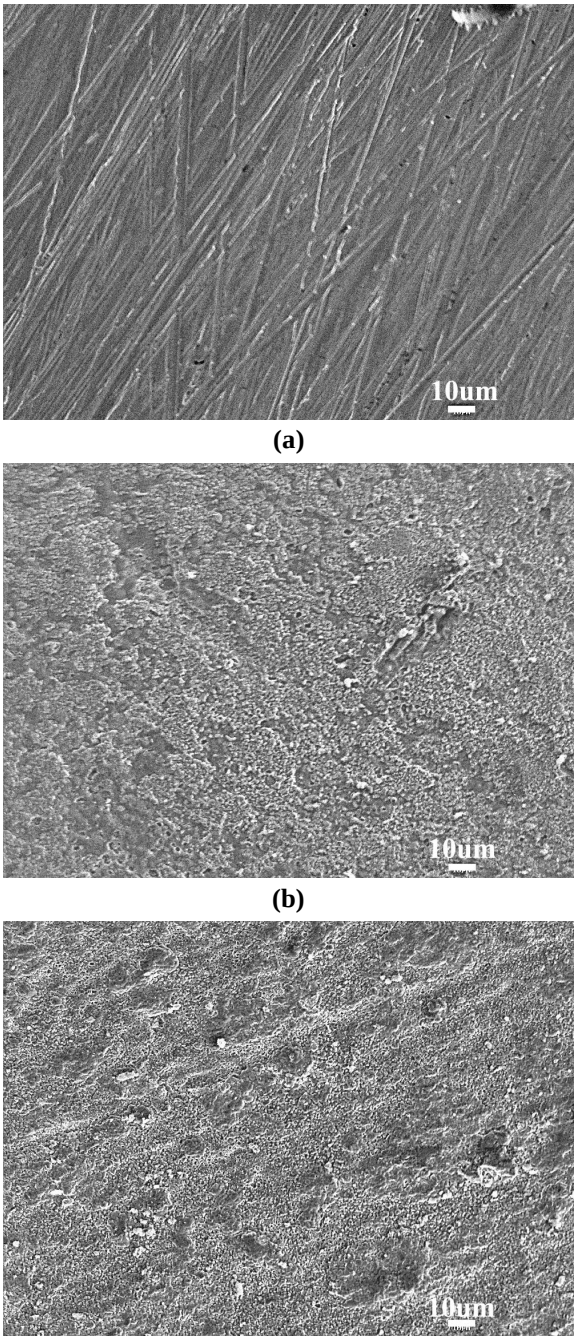

Figure 4.21: SEM morphologies of the scratched Inconel substrates before (a) and after heat treatment at 1100°C (b), and the unscratched substrate after heat treatment at 1100°C (c). The scale bar is 10 μm.

current reaches 0.01 μA. The CNT bundles grown from the pre-scratched substrate have the smallest turn-on field E_{to} = 4.2 V/μm. This may attribute to the small screen effect. Compared with the CNT forests obtained on unscratched substrate, these CNT bundles act as separated emitters centering at the highest tube in one bundle, thus would be less affected by the screen effect. And it is interesting that the CNT bundles at central and edges of the substrate exhibited different FEE properties. The smaller turn-on field on the edges of the substrate is attributed to numerous defects on the side walls, which increases the number of emission sites. Relatively, the turn-on field difference among the CNTs on the unscratched substrates small, among which the one grown under -550V shows the highest turn-on field due to its highest CNT density.

Table 4.1: FEE performances of different samples.

samples	E_{to} (V/μm)	field enhancement factor β
sample on pre-scratched substrate (center)	4.2	952
sample on pre-scratched substrate (edge)	4.03	984
sample on un-scratched substrate (-550V)	4.82	866
sample on un-scratched substrate (-500V)	4.66	872
sample on un-scratched substrate (-450V)	4.6	858
sample on un-scratched substrate (-400V)	4.6	860
sample on un-scratched substrate (+150V)	4.58	864

CHAPTER 5

CONCLUSIONS AND FUTURE WORK

Hot filament CVD was employed to investigate the direct growth of carbon nanotubes on Inconel substrates in this research. The effect of the pre-treatment temperature, substrate roughness, carbon concentration and growth bias on the growth of CNTs and field emission properties of the resultant CNTs were studied. Consequently, secondary growth of carbon nanotubes and direct synthesis of well aligned CNTs with improved FEE properties without any addition of catalyst were achieved. The main conclusions drawn from the results prescribed in Chapter 4 are summarized in this chapter. In addition, a prospective view of the future research works is also provided.

5.1 Summary and Conclusions

Time and money–consuming post-processing are normally required for the CNTs grown on substrates coated with catalyst for many applications, e.g., field emitters. Therefore, CNT grown directly on the substrate is of great significance. Direct growth of carbon nanotubes on Inconel sheets without the addition of any catalysts was achieved through a pre-oxidation treatment to the substrates. The pre-treated substrates and the resultant CNTs were characterized by SEM, XRD, TEM and FEE measurements. The main conclusions are as follows:

1. The effect of the pre-oxidation temperature, ranging from 800°C to 1100°C, on the direct growth and FEE of CNTs on Inconel sheets was studied. The results show that high temperature oxidation pre-treatment of the Inconel substrate is effective in enhancing the CNT growth and that high treatment temperature results in improved CNT uniformity and thus better field electron emission properties (lower turn-on

field and larger field enhancement factor).

2. A simple two-step deposition method, in which the primary CNTs were synthesized at extremely low carbon concentration (0.28 vol.%), and secondary growth was carried out by simply increasing the carbon concentration to 5 vol.%, was developed to grow secondary CNTs on primary ones without the addition of any catalysts throughout the whole process. The small diameter of the secondary CNTs significantly improved the FEE properties of the double–layered CNTs. Metal dusting due to low carbon concentration provides catalyst particles in the walls of primary CNTs to catalyze the secondary CNT growth.

3. The effect of bias voltages and substrate scratching before the heat treatment on the alignment of CNTs was investigated. Well aligned CNTs were synthesized by bias–enhanced HFCVD. The results show that CNTs grown under bias of -500V generates the best alignment. Aligned and non-aligned CNTs grew simultaneously on unscratched sheets in one single growth process, whereas only aligned CNTs were observed on scratched sheets at the early growth stage. Analysis shows that tip growth is not necessary for the electric field to align the CNTs, and large catalyst particles created by scratching before the heat treatment can result in alignment of CNTs at the early growth stage. In addition, tree-like CNT bundles grown on scratched substrates exhibit better FEE performances than dense carbon nanotube forest grown on unscratched substrates due to the reduced screen effect.

5.2 Future work

While direct CNT growth on Inconel has been successful, one of the future research directions is to enlarge the pool of substrates. Substrates like Ni, Fe, stainless steels, and other alloys may be employed and the results can be compared, which can provide more complete data for practical applications.

In this thesis, secondary CNT was successfully synthesized on randomly distributed CNTs. Future research can extend to the branching growth on aligned CNTs. FEE tests can be done on diverse secondary CNT structures and the results can be compared. In addition, various composites can be synthesized based on the synthesized CNT matrix. A typical example is synthesizing Cu/CNT composite by sputtering copper onto the multi-branched aligned CNT arrays for high thermal conductivity and low coefficient of thermal expansion. Future research may also focus on exploring other properties for various applications, for example, electrochemical properties.

REFERENCES

[1] C. E. Baddour and C. Briens, "Carbon nanotube synthesis: a review," *International Journal of Chemical Reactor Engineering*, vol. 3, pp. 1–18, 2005.

[2] N. Wang and B. D. Yao, "Nucleation and growth of well-aligned, uniform-sized carbon nanotubes by microwave plasma chemical vapor depositon," *Applied Physics Letters*, vol. 78, no. 25, pp. 4028–4030, June 2001.

[3] L. K.-M. P. Tribolet, "Carbon nanofibers grown on metallic filters as novel catalytic materials," *Catalysis Today*, vol. 102-103, pp. 15–22, 2005.

[4] D. Park, Y. H. Kim, and J. K. Lee, "Synthesis of carbon nanotubes on metallic substrates by a sequential combination of pecvd and thermal cvd," *Carbon*, vol. 41, no. 5, pp. 1025–1029, 2003.

[5] R. L. Vander Wal and L. J. Hall, "Carbon nanotube synthesis upon stainless steel meshes," *Carbon*, vol. 41, no. 4, pp. 659–672, 2003.

[6] M. Karwa, Z. Iqbal, and S. Mitra, "Scaled-up self-assembly of carbon nanotubes inside long stainless steel tubing," *Carbon*, vol. 44, no. 7, pp. 1235–1242, June 2006.

[7] C.-L. Lin, C.-F. Chen, and S.-C. Shi, "Field emission properties of aligned carbon nanotubes grown on stainless steel using ch4/co2 reactant gas," *Diamond and Related Materials*, vol. 13, no. 4-8, pp. 1026–1031, 2004.

[8] M. Okai, T. Muneyoshi, T. Yaguchi, and S. Sasaki, "Structure of carbon nanotubes grown by microwave-plasma-enhanced chemical vapor deposition," *Applied Physics Letters*, vol. 77, no. 21, pp. 3468–3470, Nov. 2000.

[9] N. Hirakawa, S. Sonoda, C. Tanaka, H. Murakami, and H. Yamakawa, "Electron emission properties of carbon nanotubes," *Applied Surface Science*, vol. 169, pp. 662–665, Jan. 2001.

[10] Q. Yang, Y. Tang, S. Yang, Y. Li, and A. Hirose, "Simultaneous growth of diamond thin films and carbon nanotubes at temperatures ¡= 550 degrees c," *Carbon*, vol. 46, no. 4, pp. 589–595, Apr. 2008.

[11] S. Talapatra, S. Kar, S. Pall, R. Vajtai, L. Ci, P. Victor, M. Shaijumon, S. Kaur, O. Nalamasu, and P. Ajayan, "Direct growth of aligned carbon nanotubes on bulk metals," *Nature Nanotechnology*, vol. 1, pp. 112–116, 2006.

[12] L. Gao, A. Peng, Z. Y. Wang, H. Zhang, Z. Shi, Z. Gu, G. Cao, and B. Ding, "Growth of aligned carbon nanotube arrays on metallic substrates and its application to supercapacitors," *Solid State Communications*, vol. 146, pp. 380–383, 2008.

[13] C. K. Tan, K. P. Loh, and T. T. L. John, "Direct amperometric detection of glucose on a multiple-branching carbon nanotube forest," *Analyst*, vol. 133, no. 4, pp. 448–451, 2008.

[14] N. Li, X. Chen, L. Stoica, W. Xia, J. Qian, J. Aβmann, W. Schuhmann, and M. Muhler, "The catalytic synthesis of three-dimensional hierarchical carbon nanotube composites with high electrical conductivity based on electrochemical iron deposition," *Advanced Materials*, vol. 19, no. 19, pp. 2957–2960, Oct. 2007.

[15] W. Xia, X. Chen, S. Kundu, X. Wang, G. Grundmeier, Y. Wang, M. Bron, W. Schuhmann, and M. Muhler, "Chemical vapor synthesis of secondary carbon nanotubes catalyzed by iron nanoparticles electrodeposited on primary carbon nanotubes," *Surface and Coating Technology*, vol. 201, no. 22-23, pp. 9232–9237, Sept. 2007.

[16] C. Klinke, E. Delvigne, J. Barth, and K. Kern, "Enhanced field emission from multiwall carbon nanotube films by secondary growth," *Journal of Physical Chemistry B*, vol. 109, no. 46, pp. 21 677–21 680, Nov. 2005.

[17] H. Kurachi, S. Uemura, J. Yotani, T. Nagasako, H. Yamada, T. Ezaki, T. Maesoba, T. Nakao, M. Ito, A. Sakurai, H. Shimoda, Y. Saito, and H. Shinohara, "Formation of secondary thin carbon nanotubes on thick ones and improvement in field-emission uniformity," *Japanese Journal of Applied Physics Part 1-Regular Papers Brief Communications and Review Papers*, vol. 45, no. 6A, pp. 5307–5310, June 2006.

[18] T. Kyotani, L. fu Tsai, and A. Tomita, "Formation of ultrafine carbon tubes by using an anodic aluminum oxide film as a template," *Chemistry of Materials*, vol. 7, no. 8, pp. 1427–1428, Aug. 1995.

[19] G. Che, B. B. Lakshmi, E. R. Fisher, and C. R. Martin, "Carbon nanotubule membranes for electrochemical energy storage and production," *Nature*, vol. 393, no. 6683, pp. 346–349, May 1998.

[20] S. Fan, M. G. Chapline, N. R. Franklin, T. W. Tombler, A. M. Cassell, and H. Dai, "Self-oriented regular arrays of carbon nanotubes and their field emission properties," *Science*, vol. 283, no. 5402, pp. 512–514, Jan. 1999.

[21] C. Bower, W. Zhu, S. Jin, and O. Zhou, "Plasma-induced alignment of carbon nanotubes," *Applied Physics Letters*, vol. 77, no. 6, pp. 830–832, Aug. 2000.

[22] Y. Zhang, A. Chang, J. Cao, Q. Wang, W. Kim, Y. Li, N. Morris, E. Yenilmez, J. Kong, and H. Dai, "Electric-field-directed growth of aligned single-walled carbon nanotubes," *Applied Physics Letters*, vol. 79, no. 19, pp. 3155–3157, Nov. 2001.

[23] V. I. Merkulov, D. H. Lowndes, Y. Y. Wei, and G. Eres, "Patterned growth of individual and multiple vertically aligned carbon nanofibers," *Applied Physics Letters*, vol. 76, no. 24, pp. 3555–3557, June 2000.

[24] V. I. Merkulov, A. V. Melechko, M. A. Guillorn, D. H. Lowndes, and M. L. Simpson, "Alignment mechanism of carbon nanofibers produced by plasma-enhanced chemical-vapor deposition," *Applied Physics Letters*, vol. 79, no. 18, pp. 2970–2972, Oct. 2001.

[25] V. I. Merkulov, A. V. Melechko, M. A. Guillorn, M. L. Simpson, D. H. Lowndes, J. H. Whealton, and R. J. Raridon, "Controlled alignment of carbon nanofibers in a large-scale synthesis process," *Applied Physics Letters*, vol. 80, no. 25, pp. 4816–4818, June 2002.

[26] C. Bower, O. Zhou, W. Zhu, D. J. Werder, and S. Jin, "Nucleation and growth of carbon nanotubes by microwave plasma chemical vapor deposition," *Applied Physics Letters*, vol. 77, no. 17, pp. 2767–2769, Oct. 2000.

[27] Z. F. Ren, Z. P. Huang, J. W. Xu, J. H. Wang, P. Bush, M. P. Siegal, and P. N. Provencio, "Synthesis of large arrays of well-aligned carbon nanotubes on glass," *Science*, vol. 282, no. 5391, pp. 1105–1107, Nov. 1998.

[28] Z. F. Ren, Z. P. Huang, D. Z. Wang, J. G. Wen, J. W. Xu, J. H. Wang, L. E. Calvet, J. Chen, J. F. Klemic, and M. A. Reed, "Growth of a single freestanding multiwall carbon nanotube on each nanonickel dot," *Applied Physics Letters*, vol. 75, no. 8, pp. 1086–1088, Aug. 1999.

[29] Y. Chen, Z. L. Wang, J. S. Yin, D. J. Johnson, and R. H. Prince, "Well-aligned graphitic nanofibers synthesized by plasma-assisted chemical vapor deposition," *Chemical Physics Letters*, vol. 272, no. 3-4, pp. 178–182, June 1997.

[30] Y. Chen, D. T. Shaw, and L. Guo, "Field emission of different oriented carbon nanotubes," *Applied Physics Letters*, vol. 76, no. 17, pp. 2469–2417, Apr. 2000.

[31] S. Bandow, A. Rao, K. Williams, A. Thess, R. Smalley, and P. Eklund, "Purification of single-wall carbon nanotubes by microfiltration," *Journal of Physical Chemistry B*, vol. 101, no. 44, pp. 8839–8842, Oct. 1997.

[32] R. Andrews, D. Jacques, A. Rao, F. Derbyshire, D. Qian, X. Fan, E. Dickey, and J. Chen, "Continuous production of aligned carbon nanotubes: a step closer to commercial realization," *Chemical Physics Letters*, vol. 303, no. 5-6, pp. 467–474, Apr. 1999.

[33] L. Chen, C. Wen, C. Liang, W. Hong, K. Chen, H. Cheng, C. Shen, C. Wu, and K. Chen, "Controlling steps during early stages of the aligned growth of carbon nanotubes using microwave plasma enhanced chemical vapor deposition," *Advanced Functional Materials*, vol. 12, no. 10, pp. 687–692, Oct. 2002.

[34] R. Andrews, D. Jacques, D. Qian, and E. Dickey, "Purification and structural annealing of multiwalled carbon nanotubes at graphitization temperatures," *Carbon*, vol. 39, no. 11, pp. 1681–1687, 2001.

[35] D. Luzzi and B. Smith, "Carbon cage structures in single wall carbon nanotubes: a new class of materials," *Carbon*, vol. 38, no. 11-12, pp. 1751–1756, 2000.

[36] C. Lee, S. Lyu, H. Kim, J. Lee, and K. Cho, "Synthesis of bamboo-shaped carbon-nitrogen nanotubes using $c_2h_2-nh_3-fe(co)(5)$ system," *Chemical Physics Letters*, vol. 359, no. 1-2, pp. 115–120, 2002.

[37] Q. Yang, C. Xiao, W. Chen, and A. Hirose, "Selective growth of diamond and carbon nanostructures by hot filament chemical vapor deposition," *Diamond and Related Materials*, vol. 13, pp. 433–437, 2004.

[38] A. Hartschuh, H. Pedrosa, L. Novotny, and T. Krauss, "Simultaneous fluorescence and raman scattering from single carbon nanotubes," *Science*, vol. 301, no. 5638, pp. 1354–1356, 2003.

[39] P. Lambin, A. Loiseau, C. Culot, and L. P. Biro, "Structure of carbon nanotubes probed by local and global probes," *Carbon*, vol. 40, no. 10, pp. 1635–1648, 2002.

[40] A. Thess, R. Lee, P. Nikolaev, H. Dai, P. Petit, J. Robert, C. Xu, Y. H. Lee, S. G. Kim, A. G. Rinzler, D. T. Colbert, G. E. Scuseria, D. Tomanek, J. E. Fischer, and R. E. Smalley, "Crystalline ropes of metallic carbon nanotubes," *Science*, vol. 273, no. 5274, pp. 483–487, July 1996.

[41] S. Iijima, "Helical microtubules of graphitic carbon," *Applied Physics Letters*, vol. 354, no. 6348, pp. 56–58, Nov. 1991.

[42] M. Dresslhaus, G. Dresselhaus, and P. Eklund, *Science of Fullerenes and Carbon Nanotubes*. San Diego: Academic Press, 1996.

[43] R. Saito, M. Fujita, G. Dresselhaus, and M. S. Dresselhaus, "Electronic-structure of chiral graphene tubules," *Applied Physics Letters*, vol. 60, no. 18, pp. 2204–2206, May 1992.

[44] J. W. Mintmire, B. I. Dunlap, and C. T. White, "Are fullerene tubules metallic," *Physical Review Letters*, vol. 68, no. 5, pp. 631–634, Feb. 1992.

[45] X. Blase, L. X. Benedict, E. L. Shirley, and S. G. Louie, "Hybridization effects and metallicity in small radius carbon nanotubes," vol. 72, no. 12, pp. 1878–1881, Mar. 1994.

[46] M. Bockrath, D. H. Cobden, P. L. McEuen, N. G. Chopra, A. Zettl, A. Thess, and R. E. Smalley, "Single-electron transport in ropes of carbon nanotubes," *Science*, vol. 275, no. 5308, pp. 1922–1925, Mar. 1997.

[47] S. J. Tans, M. H. Devoret, H. Dai, A. Thess, R. E. Smalley, L. J. Geerligs, and C. Dekker, "Individual single-wall carbon nanotubes as quantum wires," *Nature*, vol. 386, no. 6624, pp. 474–477, Apr. 1997.

[48] S. Frank, P. Poncharal, Z. L. Wang, and W. A. de Heer, "Carbon nanotube quantum resistors," *Science*, vol. 280, no. 5370, pp. 1744–1746, June 1998.

[49] P. Lambin, A. Fonseca, J. P. Vigneron, J. B. Nagy, and A. A. Lucas, "Structural and electronic properties of bent carbon nanotubes," *Chemical Physics Letters*, vol. 245, no. 1, pp. 85–89, Oct. 1995.

[50] L. Chico, V. H. Crespi, L. X. Benedict, S. G. Louie, and M. L. Cohen, "Pure carbon nanoscale devices: Nanotube heterojunctions," *Physical Review Letters*, vol. 76, no. 6, pp. 971–974, Feb. 1996.

[51] J. C. Charlier, T. W. Ebbesen, and P. lambin, "Structural and electronic properties of pentagon-heptagon pair defects in carbon nanotubes," *Physical Review B*, vol. 53, no. 16, pp. 11 108 –11 113, Apr. 1996.

[52] H. J. Choi, J. Ihm, S. G. Louie, and M. L. Cohen, "Defects, quasibound states, and quantum conductance in metallic carbon nanotubes," *Physical Review Letters*, vol. 84, no. 13, pp. 2917–2920, Mar. 2000.

[53] J.-M. Bonard, H. Kind, T. Stockli, and L.-O. Nilsson, "Field emission from carbon nanotubes: the first five years," *Solid State Electronics*, vol. 45, no. 6, pp. 893–914, June 2001.

[54] S. J. Tans, A. R. M. Verschueren, and C. Dekker, "Room-temperature transistor based on a single carbon nanotube," *Nature*, vol. 393, no. 6680, pp. 49–52, May 1998.

[55] R. Martel, T. Schmidt, H. R. Shea, T. Hertel, and P. Avourisa, "Single- and multi-wall carbon nanotube field-effect transistors," *Applied Physics Letters*, vol. 73, no. 17, pp. 2447–2449, Oct. 1998.

[56] M. S. Fuhrer, J. Nygard, L. Shih, M. Forero, Y.-G. Yoon, M. S. C. Mazzoni, H. J. Choi, J. Ihm, S. G. Louie, A. Zettl, and P. L. McEuen, "Crossed nanotube junctions," *Science*, vol. 288, no. 5465, pp. 494–497, Apr. 2000.

[57] B. T. Kelly, *Physics of Graphite*. London: Applied Science, 1981.

[58] J. Lu and J. Han, "Carbon nanotubes and nanotube-based nano devices," *International Journal of High Speed Electronics and Systems*, vol. 9, pp. 101–123, 1998.

[59] J. P. Lu, "Elastic properties of carbon nanotubes and nanoropes," *Physical Review Letters*, vol. 79, no. 7, pp. 1297–1300, Aug. 1997.

[60] M. Treacy, T. Ebbesen, and J. Gibson, "Exceptionally high young's modulus observed for individual carbon nanotubes," *nature*, vol. 381, no. 6584, pp. 678–680, June 1996.

[61] E. Wong, P. Sheehan, and C. Lieber, "Nanobeam mechanics: Elasticity, strength, and toughness of nanorods and nanotubes," *Science*, vol. 277, no. 5334, pp. 1971–1975, Sept. 1997.

[62] J. P. Salvetat, J. M. Bonard, N. Thomson, A. Kulik, L. Forro, W. Benoit, and L. Zuppiroli, "Mechanical properties of carbon nanotubes," *Applied Physics A-Materials science and processing*, vol. 69, no. 3, pp. 255–260, July 1999.

[63] H. Dai, J. H. Hafner, A. G. Rinzler, D. T. Colbert, and R. E. Smalley, "Nanotubes as nanoprobes in scanning probe microscopy," *Nature*, vol. 384, no. 6605, pp. 147–150, Nov. 1996.

[64] R. M. D. Stevens, N. A. Frederick, B. L. Smith, D. E. Morse, G. D. Stucky, and P. K. Hansma, "Carbon nanotubes as probes for atomic force microscopy," *Nanotechnology*, vol. 11, no. 1, pp. 1–5, Mar. 2000.

[65] R. Heyd, A. Charlier, and E. McRae, "Uniaxial-stress effects on the electronic properties of carbon nanotubes," *Physical Review B*, vol. 55, no. 11, pp. 6820–6824, Mar. 1997.

[66] L. Yang, M. P. Anantram, J. Han, and J. P. Lu, "Band-gap change of carbon nanotubes: Effect of small uniaxial and torsional strain," *Physical Review B*, vol. 60, no. 19, pp. 13 874–13 878, Nov. 1999.

[67] T. W. Tombler, C. Zhou, L. Alexseyev, J. Kong, H. Dai, L. Liu, C. S. Jayanthi, M. Tang, and S.-Y. Wu, "Reversible electromechanical characteristics of carbon nanotubes under local-probe manipulation," *Nature*, vol. 405, no. 6788, pp. 769–772, June 2000.

[68] R. H. Baughman, C. Cui, A. A. Zakhidov, Z. Iqbal, J. N. Barisci, G. M. Spinks, G. G. Wallace, A. Mazzoldi, D. D. Rossi, A. G. Rinzler, O. Jaschinski, S. Roth, and M. Kertesz, "Carbon nanotube actuators," *Science*, vol. 284, no. 5418, pp. 1340–1344, May 1999.

[69] A. M. Rao, E. Richter, S. Bandow, B. Chase, P. C. Eklund, K. A. Williams, S. Fang, K. R. Subbaswamy, M. Menon, A. Thess, R. E. Smalley, G. Dresselhaus, and M. S. Dresselhaus, "Diameter-selective raman scattering from vibrational modes in carbon nanotubes," *Science*, vol. 275, no. 5297, pp. 187–191, Jan. 1997.

[70] S. M. Bachilo, M. S. Strano, C. Kittrell, R. H. Hauge, R. E. Smalley, and R. B. Weisman, "Structure-assigned optical spectra of single-walled carbon nanotubes," *Science*, vol. 298, no. 5602, pp. 2361–2366, Dec. 2002.

[71] M. Freitag, Y. Martin, J. A. Misewich, R. Martel, and P. Avouris, "Photoconductivity of single carbon nanotubes," *Nano Letters*, vol. 3, no. 8, pp. 1067–1071, Aug. 2003.

[72] J. A. Misewich, R. Martel, P. Avouris, J. C. Tsang, S. Heinze, and J. Tersoff, "Electrically induced optical emission from a carbon nanotube fet," *Science*, vol. 300, no. 5620, pp. 783–786, May 2003.

[73] J. Heremans, C. H. Olk, and D. T. Morelli, "Magnetic susceptibility of carbon structures," *Physical Review B*, vol. 49, no. 21, pp. 15 122–15 125, June 1994.

[74] M. Fujiwara, E. Oki, M. Hamada, and Y. Tanimoto, "Magnetic orientation and magnetic properties of a single carbon nanotube," *Journal of Physical Chemistry A*, vol. 105, no. 18, pp. 4383–4386, May 2001.

[75] D. A. Walters, M. J. Casavant, X. C. Qin, C. B. Huffman, P. J. Boul, L. M. Ericson, E. H. Haroz, M. J. O'Connell, K. Smith, D. T. Colbert, and R. E. Smalley, "In-plane-aligned membranes of carbon nanotubes," *Chemical Physics Letters*, vol. 338, no. 1, pp. 14–20, Apr. 2001.

[76] L. Yang and J. Han, "Electronic structure of deformed carbon nanotubes," *Physical Review Letters*, vol. 85, no. 1, pp. 154–157, July 2000.

[77] S. C. Tsang, Y. K. Chen, P. J. F. Harris, and M. L. H. Green, "A simple chemical method of opening and filling carbon nanotubes," *Nature*, vol. 372, no. 6502, pp. 159–162, Nov. 1994.

[78] P. M. Ajayan, O. Stephan, P. Redlich, and C. Colliex, "Carbon nanotubes as removable templates for metal oxide nanocomposites and nanostructures," *Nature*, vol. 375, no. 6532, pp. 564–567, June 1995.

[79] D. Ugarte, A. Chatelain, and W. A. de Heer, "Nanocapillarity and chemistry in carbon nanotubes," *Science*, vol. 274, no. 5294, pp. 1897–1899, Dec. 1996.

[80] N. Rajalakshmi, K. S. Dhathathreyan, A. Govindaraj, and B. C. Satishkumar, "Electrochemical investigation of single-walled carbon nanotubes for hydrogen storage," *Electrochimica Acta*, vol. 45, no. 27, pp. 4511–4515, 2000.

[81] J. Zhao, A. Buldum, J. Han, and J. P. Lu, "Gas molecule adsorption in carbon nanotubes and nanotube bundles," *Nanotechnology*, vol. 13, no. 2, pp. 195–200, Apr. 2002.

[82] B. Gao, C. Bower, J. D. Lorentzen, L. Fleming, A. Kleinhammes, X. P. Tang, L. E. McNeil, Y. Wu, and O. Zhou, "Enhanced saturation lithium composition in ball-milled single-walled carbon nanotubes," *Chemical Physics Letters*, vol. 327, no. 1-2, pp. 69–75, Sept. 2000.

[83] E. Frackowiak, K. Jurewicz, S. Delpeux, and F. Beguin, "Nanotubular materials for supercapacitors," *Journal of Power Sources*, vol. 97-8, pp. 822–825, July 2001.

[84] S. Iijima and T. Ichihashi, "Single-shell carbon nanotubes of 1-nm diameter," *Nature*, vol. 363, no. 6430, pp. 603–605, June 1993.

[85] H. Dai, *Carbon Nanotubes*, ser. Topics in Applied Physics. Springer-Verlag Berlin Heidelberg, 2001, vol. 80, ch. Nanotube growth and characterization, pp. 29–53.

[86] T. Guo, P. Nikolaev, A. Thess, D. Colbert, and R. Smalley, "Catalytic growth of single-walled manotubes by laser vaporization," *Chemical Physics Letters*, vol. 243, no. 1-2, pp. 49–54, Sept. 1995.

[87] M. Jose-Yacaman, M. Miki-Yoshida, L. Rendon, and J. G. Santiesteban, "Catalytic growth of carbon microtubules with fullerene structure," *Applied Physics Letters*, vol. 62, no. 2, pp. 202–204, Jan. 1993.

[88] V. Ivanov, J. B. Nagy, P. Lambin, A. Lucas, X. B. Zhang, X. F. Zhang, D. Bernaerts, G. V. Tendeloo, S. Amelinckx, and J. V. Landuyt, "The study of carbon nanotubules produced by catalytic method," *Chemical Physics Letters*, vol. 223, no. 4, pp. 329–335, June 1994.

[89] S. Amelinckx, X. B. Zhang, D. Bernaerts, X. F. Zhang, V. Ivanov, and J. B. Nagy, "A formation mechanism for catalytically grown helix-shaped graphite nanotubes," *Science*, vol. 265, no. 5172, pp. 635–639, July 1994.

[90] M.Meyyappan, *Carbon Nanotubes: Science and Applications*. CRC Press Inc, 2005, ch. Growth:CVD and PECVD, pp. 99–112.

[91] A. Cassell, J. Raymakers, J. Kong, and H. Dai, "Large scale cvd synthesis of single-walled carbon nanotubes," *Journal of Physical Chemistry B*, vol. 103, no. 31, pp. 6484–6492, Aug. 1999.

[92] M. J. Bronikowski, P. A. Willis, D. T. Colbert, K. A. Smith, and R. E. Smalley, "Gas-phase production of carbon single-walled nanotubes from carbon monoxide via the hipco process: A parametric study," *Journal of Vacuum Science and Technology A-Vacuum Surfaces and Films*, vol. 19, no. 4, pp. 1800–1805, July 2001.

[93] M. Endo, K. Takeuchi, S. Igarashi, K. Kobori, M. Shiraishi, and H. W. Kroto, "The production and structure of pyrolytic carbon nanotubes (pcnts)," *Journal of Physics and Chemistry of Solids*, vol. 54, no. 12, pp. 1841–1848, Dec. 1993.

[94] H. Kanzow and A. Ding, "Formation mechanism of single-wall carbon nanotubes on liquid-metal particles," *Physical Review B*, vol. 60, no. 15, pp. 11 180–11 186, Oct. 1999.

[95] A. H. Mahan, J. L. Alleman, M. J. Heben, P. A. Parilla, K. M. Jones, and A. C. Dillon, "Hot wire chemical vapor deposition of isolated carbon single-walled nanotubes," *Applied Physics Letters*, vol. 81, no. 21, pp. 4061–4063, Nov. 2002.

[96] J. Kong, C. Zhou, A. Morpurgo, H. Soh, C. Quate, C. Marcus, and H. Dai, "Synthesis, integration, and electrical properties of individual single-walled carbon nanotubes," *Applied Physics A-Materials science and processing*, vol. 69, no. 3, pp. 305–308, Sept. 1999.

[97] L. Marty, V. Bouchiat, A. Bonnot, M. Chaumont, T. Fournier, S. Decossas, and S. Roche, "Batch processing of nanometer-scale electrical circuitry based on in-situ grown single-walled carbon nanotubes," *Mircoelectronic Engineering*, vol. 61-2, pp. 485–489, July 2002.

[98] M. Chhowalla, K. B. K. Teo, C. Ducati, N. L. Rupesinghe, G. A. J. Amaratunga, A. C. Ferrari, D. Roy, J. Robertson, and W. I. Milne, "Growth process conditions of vertically aligned carbon nanotubes using plasma enhanced chemical vapor deposition," *Journal of Applied Physics*, vol. 90, no. 10, pp. 5308–5317, Nov. 2001.

[99] C. C. Lin, I. C. Leu1, J. H. Yen, and M. Hon, "Sheath-dependent orientation control of carbon nanofibres and carbon nanotubes during plasma-enhanced chemical vapour deposition," *Nanotechnology*, vol. 15, no. 1, pp. 176–179, Jan. 2004.

[100] L. Delzeit, I. McAninch, B. A. Cruden, D. Hash, B. Chen, J. Han, and M. Meyyappan, "Growth of multiwall carbon nanotubes in an inductively coupled plasma reactor," *Journal of Applied Physics*, vol. 91, no. 9, pp. 6027–6033, May 2002.

[101] S. H. Tsai, C. W. Chao, C. L. Lee, and H. C. Shih, "Bias-enhanced nucleation and growth of the aligned carbon nanotubes with open ends under microwave plasma synthesis," *Applied Physics Letters*, vol. 74, no. 23, pp. 3462–3464, June 1999.

[102] Y. C. Choi, Y. M. Shin, S. C. Lim, D. J. Bae, Y. H. Lee, B. S. Lee, and D.-C. Chung, "Effect of surface morphology of ni thin film on the growth of aligned carbon nanotubes by microwave plasma-enhanced chemical vapor deposition," *Journal of Applied Physics*, vol. 88, no. 8, pp. 4898–4903, Oct. 2000.

[103] H. Cui, O. Zhou, and B. R. Stoner, "Deposition of aligned bamboo-like carbon nanotubes via microwave plasma enhanced chemical vapor deposition," *Journal of Applied Physics*, vol. 88, no. 10, pp. 6072–6074, Nov. 2000.

[104] C. H. Lin, H. L. Chang, C. M. Hsu, A. Y. Lo, and C. T. Kuo, "The role of nitrogen in carbon nanotube formation," *Diamond and Related Materials*, vol. 12, no. 10-11, pp. 1851–1857, 2003.

[105] Q. Yang, C. Xiao, W. Chen, A. Singh1, T. Asai, and A. Hirose, "Growth mechanism and orientation control of well-aligned carbon nanotubes," *Diamond and Related Materials*, vol. 12, pp. 1482–1487, 2003.

[106] B. O. Boskovic, V. Stolojan, R. U. Khan, S. Haq, S. Ravi, and P. Silva, "Large-area synthesis of carbon nanofibres at room temperature," *Nature Materials*, vol. 1, no. 3, pp. 165–168, Nov. 2002.

[107] J. S. Suh, K. S. Jeong, J. S. Lee, and I. Han, "Study of the field-screening effect of highly ordered carbon nanotube arrays," *Applied Physics Letters*, vol. 80, no. 13, pp. 2392–2394, Apr. 2002.

[108] R. Seidel, G. Duesberg, E. Unger, A. Graham, M. Liebau, and F. Kreupl, "Chemical vapor deposition growth of single-walled carbon nanotubes at 600 degrees c and a simple growth model," *Journal of Physical Chemistry B*, vol. 108, no. 6, pp. 1888–1893, Feb. 2004.

[109] Y. Saito, M. Okuda, M. Tomita, and T. Hayashi, "Extrusion of single-wall carbon nanotubes via formation of small particles condensed near an arc evaporation source," *Chemical Physics Letters*, vol. 236, no. 4-5, pp. 419–426, Apr. 1995.

[110] P. Parthangal, R. Cavicchi, and M. Zachariah, "A generic process of growing aligned carbon nanotube arrays on metals and metal alloys," *Nanotechnology*, vol. 18, no. 18, pp. 1–5, Apr. 2007.

[111] H. Yang, P. Mercier, S. C. Wang, and D. L. Akins, "High-pressure synthesis of carbon nanotubes with a variety of morphologies," *Chemical Physics Letters*, vol. 416, no. 1-3, pp. 18–21, Nov. 2005.

[112] J. Panitz, P. Novak, and O. Haas, "Raman microscopy applied to rechargeable lithium-ion cells-steps in situ raman imaging with increased optical efficiency," *Applied Spectroscopy*, vol. 55, no. 9, pp. 1131–1137, 2001.

[113] Y. Soneda and M. Makino, "Formation and texture of carbon nanofilaments by the catalytic decomposition of co on stainless-steel plate," *Carbon*, vol. 38, no. 3, pp. 478–480, 2000.

[114] Z. Mao, A. Garg, and S. B. Sinnott, "Molecular dynamics simulations of the filling and decorating of carbon nanotubules," *Nanotechnology*, vol. 10, no. 3, pp. 273–277, Sept. 1999.

[115] M. Guillorn, X. Yang, A. Melechko, D. Hensley, M. Hale, V. Merkulov, M. Simpson, L. Baylor, W. Gardner, and D. Lowndes, "Vertically aligned carbon nanofiber-based field emission electron sources with an integrated focusing electrode," *Journal of Vacuum Science & Technology*, vol. 22, no. 1, pp. 35–39, 2004.

[116] H. Sugie, M. Tanemura, V. Filip, K. Iwata, K. Takahashi, and F. Okuyama, "Carbon nanotubes as electron source in an x-ray tube," *Applied Physics Letters*, vol. 78, no. 17, pp. 2578–2580, Apr. 2001.

[117] Q. Ye, A. Cassell, H. Liu, K. Chao, J. Han, and M. Meyyappan, "Large-scale fabrication of carbon nanotube probe tips for atomic force microscopy critical dimension imaging applications," *Nano Letters*, vol. 4, no. 7, pp. 1301–1308, July 2004.

[118] J. Li, C. Papadopoulos, J. M. Xu, and M. Moskovits, "Highly-ordered carbon nanotube arrays for electronics applications," *Applied Physics Letters*, vol. 75, no. 3, pp. 367–369, July 1999.

[119] Y. Avigal and R. Kalish, "Growth of aligned carbon nanotubes by biasing during growth," *Applied Physics Letters*, vol. 78, no. 16, pp. 2291–2293, Apr. 2001.

[120] L.-H. Chen, J. F. AuBuchon, A. Gapin, C. Daraio, P. Bandaru, S. Jin, D. W. Kim, I. K. Yoo, and C. M. Wang, "Control of carbon nanotube morphology by change of applied bias field during growth," *Applied Physics Letters*, vol. 85, no. 22, pp. 5373–5375, Nov. 2004.

[121] Z. Huang, D. Wang, J. Wen, M. Sennett, H. Gibson, and Z. Ren, "Effect of nickel, iron and cobalt on growth of aligned carbon nanotubes," *Applied Physics A-Materials science and processing*, vol. 74, no. 3, pp. 387–391, Mar. 2002.

[122] W. Xia, O. F.-K. Schlter, C. Liang, M. W. van den Berg, M. Guraya, and M. Muhler, "The synthesis of structured pd/c hydrogenation catalysts by the chemical vapor deposition of pd(ally1)cp onto functionalized carbon nanotubes anchored to vapor grown carbon microfibers," *Catalysis Today*, vol. 102, pp. 34–39, May 2005.

[123] M. Sveningsson, R. E. Morjan, O. A. Nerushev, and E. E. Campbell, "Highly efficient electron field emission from decorated multiwalled carbon nanotube films," *Applied Physics Letters*, vol. 85, no. 19, pp. 4487–4489, Nov. 2004.

[124] P. Sarazin, *Carbon Nanotubes:Science and Applications*. Boca Raton: CRC Press Inc, 2005, ch. 8.

[125] R. H. Fowler and L. Nordheim, "Electron emission in intense electric fields," in *Proceedings of the Royal Society of London*, ser. A, vol. 119. The Royal Society, May 1928, pp. 173–181.

[126] R. Forbes, "Field emission: New theory for the derivation of emission area from a fowler-nordheim plot," *Journal of Vacuum Science and Technology B*, vol. 17, no. 2, pp. 526–533, 1999.

[127] X. Lu, Q. Yang, C. Xiao, and A. Hirose, "Nonlinear fowler-nordheim plots of the field electron emission from graphitic nanocones: influence of non-uniform field enhancement factors," *Journal Of Physics D-Applied Physics*, vol. 39, no. 15, pp. 3375–3379, Aug. 2006.

[128] L. Nilsson, O. Groening, C. Emmenegger, O. Kuettel, E. Schaller, L. Schlapbach, H. Kind, J.-M. Bonard, and K. Kern, "Scanning field emission from patterned carbon nanotube films," *Applied Physics Letters*, vol. 76, no. 15, pp. 2071–2073, Apr. 2000.

[129] S. Z. Deng, N. S. Xu, J. B. Liu, J. Chen, Y. L. Ke, and J. C. She, "Field electron emission properties from aligned carbon nanotube bundles of different density," *Surface and Interface Analysis*, vol. 36, no. 5-6, pp. 501–505, 2004.

[130] M. Chhowalla, C. Ducati, N. L. Rupesinghe, K. B. K. Teo, and G. A. J. Amaratunga, "Field emission from short and stubby vertically aligned carbon nanotubes," *Applied Physics Letters*, vol. 79, no. 13, pp. 2079–2081, Sept. 2001.

[131] C. Kim, Y. S. Choi, S. M. Lee, J. T. Park, B. Kim, and Y. H. Lee, "The effect of gas adsorption on the field emission mechanism of carbon nanotubes," *Journal of the American Chemical Society*, vol. 124, no. 33, pp. 9906–9911, Aug. 2002.

[132] J.B.Wachtman, *Characterization of Materials*. Manning Press, 1993.

[133] C. Gommes, S. Blacher, K. Masenelli-Varlot, C. Bossuot, E. McRae, A. Fonseca, J. B. Nagy, and J. P. Pirar, "Image analysis characterization of multi-walled carbon nanotubes," *Carbon*, vol. 41, no. 13, pp. 2561–2572, 2003.

[134] P. K. Chu and L. Li, "Characterization of amorphous and nanocrystalline carbon films," *Materials Chemistry and Physics*, vol. 96, no. 2-3, pp. 253–277, Apr. 2006.

[135] X. Lu, "Field electron emission from diamond and related films synthesized by plasma enhanced chemical vapor deposition," Ph.D. dissertation, University of Saskatchewan, Department of Physics and Engineering Physics,Saskatoon, Saskatchewan S7N 5E2, 2006.

[136] O. Altin and S. Eser, "Pre-oxidation of inconel alloys for inhibition of carbon deposition from heated jet fuel," *Oxidation of Metals*, vol. 65, no. 1-2, pp. 75–99, 2006.

[137] L. Jian, C. Yuh, and M. Farooque, "Oxidation behavior of superalloys in oxidizing and reducing environments," *Corrosion Science*, vol. 42, pp. 1573–1585, 2000.

[138] G. Calvarin, R. Molins, and A. M. Huntz, "Oxidation mechanism of ni-20cr foils and its relation to the oxide-scale microstructure," *Oxidation of Metals*, vol. 53, no. 1-2, pp. 25–48, 2000.

[139] C. P. Deck and K. Vecchio, "Prediction of carbon nanotube grown success by the analysis of carbon-catalyst binary phase diagrams," *Carbon*, vol. 44, pp. 267–275, 2006.

[140] Z. Yu, D. Chen, B. Totdal, T. Zhao, Y. Dai, W. Yuan, and A. Holmen, "Catalytic engineering of carbon nanotube production," *Applied Catalysis A-General*, vol. 279, no. 1-2, pp. 223–233, Jan. 2005.

[141] Y. Li, X. B. Zhang, X. Y. Tao, J. M. Xu, W. Z. Huang, J. H. Luo, Z. Q. Luo, T. Li, F. Liu, Y. Bao, and H. J. Geise, "Mass production of high-quality multi-walled carbon nanotube bundles on a ni/mo/mgo catalyst," *Carbon*, vol. 43, pp. 295–301, 2005.

[142] M. D. Lima, R. Bonadiman, M. J. Andrade, J. Toniolo, and C. P. Bergmann, "Synthesis of multi-walled carbon nanotubes by catalytic chemical vapor deposition using $Cr_{2-x}Fe_xO_3$ as catalyst," *Diamond and Related Materials*, vol. 15, no. 10, pp. 1708–1713, Oct. 2006.

[143] T. Arcos, M. Garnier, J. Seo, P. Oelhafen, V. Thommen, and D. mathys, "The influence of catalyst chemical state and morphology on carbon nanotube growth," *Journal of Physical Chemistry B*, vol. 108, pp. 7728–7734, 2004.

[144] M. M. Shaijumon, N. Bejoy, and S. Ramaprabhu, "Catalytic growth of carbon nanotubes over ni/cr hydrotalcite-type anionic clay and their hydrogen storage properties," *Applied Surface Science*, vol. 242, pp. 192–198, 2005.

[145] G. Che, B. B. Lakshmi, C. R. Martin, E. R. Fisher, and R. S. Ruoff, "Chemical vapor deposition based synthesis of carbon nanotubes and nanofibers using a template method," *Chemistry of Materials*, vol. 10, pp. 260–267, 1998.

[146] X. Lu, Q. Yang, C. Xiao, and A. Hirose, "Field electron emission of carbon-based nanocone films," *Applied Physics A-Materials science and processing*, vol. 82, pp. 293–296, 2006.

[147] W. Y. Sung, J. G. Ok, W. J. Kim, S. Lee, E. Y. Jang, and Y. H. Kim, "Fabrication and the enhanced emission uniformity of carbon nanofibers using a glass cap," *Nanotechnology*, vol. 18, no. 33, pp. 1–5, Aug. 2007.

[148] P. Szakalos, R. Pettersson, and S. Hertzman, "An active corrosion mechanism for metal dusting on 304l stainless steel," *Corrosion Science*, vol. 44, no. 10, pp. 2253–2270, Oct. 2002.

[149] H. Grabke, R. Krajak, and J. N. Paz, "On the mechanism of catastrophic carburization - metal dusting," *Corrosion Science*, vol. 35, no. 5-8, pp. 1141–1150, 1993.

[150] J. Yotani, S. Uemura, T. Nagasako, H. Kurachi, H. Yamada, T. Ezaki, T. Maesoba, T. Nakao, M. Ito, T. Ishida, and Y. Saito, "Emission enhancement by excimer laser irradiation over a weblike carbon nanotube layer," *Japanese Journal of Applied Physics Part 2-Letters & Express Letters*, vol. 43, no. 11B, pp. L1459–L1462, Nov. 2004.

[151] H. Kurachi, S. Uemura, J. Yotani, T. Nagasako, H. Yamada, T. Ezaki, T. Maesoba, T. Nakao, M. Ito, A. Sakurai, Y. Saito, and H. Shinohara, "Uniform carbon-nanotube emitter for field-emission displays," *Journal of the Society for Information Display*, vol. 13, no. 9, pp. 727–733, Sept. 2005.

[152] J.-M. Bonard, N. Weiss, H. Kind, T. Stockli, L. Forro, K. Kern, and A. Chatelain, "Tuning the field emission properties of patterned carbon nanotube films," *Advanced Materials*, vol. 13, no. 3, pp. 184–188, Feb. 2001.